Numerical Simulation & Risk Analysis of Well Kick

by

© MD Rakibul Islam

A thesis submitted to

School of Graduate Studies

in partial fulfilment of the

requirements for the degree of

Master of Engineering

May 2017

Faculty of Engineering and Applied Science

Memorial University of Newfoundland

St John's Newfoundland

to my Mom & Dad

Abstract

Oil and gas development is moving into harsh and remote locations where the highest level of safety is required. A blowout is one of the most feared accidents in oil and gas developments projects, which is the result of uncontrolled flow of influx into the wellbore. Limited insights about the rapidly changing physical parameters during a blowout necessitates the exhaustive analysis of kick detection parameters. The risk of blowout consequences can be minimized by appropriate kick detection and well control techniques. This work presents a dynamic numerical simulation of kick detection and experimental studies to analyze hydrodynamic properties of drilling fluid to detect a kick. The experimental results are used to verify dynamic numerical simulation results. A three dimensional CFD simulation of a pressure cell which is a mimic of a scaled down version of a wellbore is performed using commercial CFD package ANSYS Fluent-15. The main objective of this simulation model is to analyze the pressure gradient, rising speed of a gas kick and volumetric behaviour of the gas kick with respect to time. Simulation results exhibit a sudden increase of pressure while the kick enters and volumetric expansion of gas as it flows upward. This improved understanding helps to develop effective well control strategies. The proposed numerical simulation model is validated by comparison with experimentally obtained downhole pressure during an influx into the pressure cell. This study confirms the feasibility and usability of an intelligent drill pipe as a tool to monitor well condition and develop blowout risk management strategies. Furthermore, to quantify the risk of blowout consequences, this work aims to test and validate a blowout risk assessment model using uniquely developed experimental results. Kick detection is a major

part of the blowout risk assessment model. The accuracy and timeliness of kick detection are dependent on the monitoring of multiple downhole parameters such as downhole pressure, fluid density, fluid conductivity and mass flow rate. In the present study these four parameters are considered in different logical combinations to assess the occurrence of kick and associated blowout risk. The assessed results are compared against the experimental observations. It is observed that simultaneous monitoring of mass flow rate combined with any one the three parameters provides most reliable detection of kick and potential blowout likelihood. This work confirms that a blowout risk model integrated with real time monitoring is a reliable and effective way of managing blowout risk. Upon success testing of this approach at the pilot and field levels, this approach could provide a paradigm shift in drilling safety.

Acknowledgements

I would like to express my deepest appreciation for my supervisors Dr Faisal Khan and Dr Ramchandran Venkatesan who throughout this work offered their guidance and conveyed a spirit of adventure in regard to this research. Without their persistent help and encouragement this thesis would not have been possible. In addition, I would like to express my special gratitude to Ayesha Anjuman Nayeem for developing and modeling the experimental setup, without which this work wouldn't be initiated. Moreover, I gratefully acknowledge the financial support provided by Newfoundland & Labrador and Natural Science and Engineering Research Council (NSERC) of Canada, School of Graduate Studies (SGS).

Table of Contents

List of Figures

List of Tables

Nomenclature

C_{e1}, C_{e2}	Constant for intermittency equation
C_{a1}, C_{a2}	Constant for intermittency equation
F_{length}	Empirical correlation
F_{onset}	Triggers the intermittency production
F_{turb}	Term to disable destruction/relaminarization source
E	Total energy (J)
p	Pressure (Pa)
I	Unit tensor (1/s)
k_{eff}	Effective conductivity (W/m k)
R	Universal constant (J/mol k)
m_w	Molecular weight (kg/mol)
S	Strain rate magnitude
S_{cav}	Mass transfer between two phases
T	Temperature (k)
V	Volume (m^3)

Greek letters

α	Volume fraction
μ	Dynamic viscosity (Pa s)
$\bar{\bar{\tau}}$	Stress tensor (kg/ms^2)
ρ	Density of fluid (kg/m^3)
λ	Bulk viscosity coefficient
γ	Intermittency
Ω	Vorticity magnitude

Vectors

$\vec{F}$	Force vector from source term (N)

$\vec{v}$ Overall velocity vector (m/s)

$\vec{g}$ Gravitational acceleration (m/s^2)

Operators

$\frac{\partial}{\partial t}$ Partial time derivative (s^{-1})

$\nabla.$ Divergence operator (m^{-1})

T Transpose of a tensor

Abbreviations

SCFM…… Standard Cubic Feet per Minute

BHP……. Bottom Hole Pressure

CDF……Cumulative Distribution Function

CFD…… Computational Fluid Dynamics

RANS……. Reynold Averaged Navier Stokes

FVM……. Finite Volume Method

Chapter 1

1 Introduction

The demand of rising energy is boosting oil exploration to harsh and remote environment. However, several safety issues are integrated during oil exploration and drilling in deepwater. Blowout is recognized as the most devastating consequence in deepwater drilling. An influx or kick into the wellbore is known as the initiating event of blowout consequences. The recent BP Deepwater Horizon accident significantly raised the concern about the safety and integrity of oil exploration in deepwater. The loss of life and consequences could have been avoided if timely and adequate preventions were taken. Risk based decision making and continuous risk assessment could have minimized the devastating consequences. Though the risk of blowout can be manageable upon proper detection of kick and well control techniques but the continuous campaign of drilling to the remotest and hostile environments is increasing the challenge of kick detection and well control techniques.

1.1 Why Risk Assessment?

Risk assessment is the process of thorough investigation to identify the hazards for evaluating the risk associated with hazard. Determination of the appropriate control procedure to minimize the associated risk is also considered as a part of risk assessment. Risk assessment model is considered as an integral part of process design to determine

whether acceptable precaution is taken to minimize the risk. To develop a strategy for preventing accident and safety related decision making risk analysis is used as a tool. Most of the major accident that occur in oil and gas industry each year result from a series of unwanted events. Series of accidents can lead to deaths, environmental consequences and property destruction. These types of vulnerabilities and undesired events can be identified sequentially when a systematic and organized risk assessment tools and techniques are combined. Applying the rules of probability theory, probabilistic risk assessment can be carried out to mitigate or reduce the risk. Further progress on risk assessment model can be possible when other tools such as failure mode and effective analysis (FMEA) and fault tree analysis (FTA) are incorporated in design. FMEA is a proactive method where sequential analysis are performed to determine the modes of failure, the causes of failure and the effects of failure. The main purpose of FMEA is to take necessary action to eliminate the failure starting from the one with highest priority. Fault tree analysis is a systematic and logical safety analysis tool where the undesired event proceeds through the logical combinations to the root causes of that event. Logical operator OR and AND gates are used to link the undesired events to its root causes.

1.2 Significance of Numerical Simulation

Computational fluid dynamics is a numerical method of solving the mathematical equations using high performance computer that defines the behaviour of fluid and gas flow. Computational fluid dynamics is embraced by researchers and industries to obtain measurable improvements in innovation. Based on this approach, diversified

hydrodynamic behaviour of fluid can be studied in a cost effective way. Furthermore, detailed insights into the system that may not be able to understand through experimentally, can be achieved and visualized by CFD simulations. To optimize the efficiency of a product or process, prediction and controlling of fluid flow is performed by using numerous commercial software. The usability of simulation studies are increasing because of the capacity to study a system under unlimited boundary conditions. Numerous commercial CFD software packages have been developed considering the level of requirement and complexity of model. Autodesk flow design is developed for simulation of simple model. Though this tool is quite renowned for simplicity in use but comes with the shortcomings of user defined solver methods and models. To analyze the complicated flow simulation such as fluid structure interaction, free surface flow, flowing of chemical solution through pores, ANSYS CFX, ANSYS Fluent and OpenFOAM are widely used. These software enable users to define several solver methods according to the requirement. Now a days the CFD tools are considered essential and necessary for tasks such as combustion research, multiphase flow simulation etc.

1.3 Objectives

The key goals of this research work are described below:

- To develop a numerical simulation model based on computational fluid dynamics. Commercial CFD package ANSYS Fluent-15 is used to develop the numerical model.

- Validation and comparison of the proposed numerical model with experimental results. The experimental observations are obtained by conducting experiment on a uniquely developed experimental setup

- Analysis of the hydrodynamic property of drilling fluid such as pressure gradient, rising speed of gas kick and volumetric behaviour of gas kick with respect to time. Exhaustive analysis of simulation results are performed to study the hydrodynamic property.

- To propose a blowout risk assessment model and methodology where experimental data will be taken in consideration for quantitative study of blowout consequences. Bowtie approach is adapted to develop the desired risk assessment model. Several runs of experiments are conducted using the pre-developed experimental setup.

- To validate kick detection part of the risk assessment model. Experimental failure probability is calculated to validate the risk assessment model.

- To integrate the validated model in risk assessment model for quantification of blowout risk.

- Time dependency analysis of the proposed model to obtain real time assessment of risk. The experimental runs are segmented in different time windows to analyze the time dependency.

1.4 Contributions

The main contributions of this thesis are listed below:

- A numerical simulation model based on commercial CFD package is proposed for exhaustive analysis of hydrodynamic behaviour of drilling fluid during a gas kick.
- The proposed numerical model is validated and compared with experimentally obtained results. The validated numerical model can be further extended for studying the hydrodynamic behaviour of drilling fluid in full scale wellbore.
- A blowout risk assessment model is proposed based on kick detection and consequences as a functions of incident and well control barriers.
- The proposed risk assessment model is validated and tested with uniquely developed experimental results. The developed risk assessment model and methodology can be practically implemented for on time risk assessment and decision making. The visualization and real time quantification of risk is possible when the proposed model is logically coded and integrated with required software.

1.5 Thesis Outline

- **Chapter 1:** This chapter introduces the research topic and focuses on the motivation of the work. The key objectives and expected outcomes of this work are briefly explained in this chapter.
- **Chapter 2:** This chapter illustrates a detailed overview on the causes of blowout and well control techniques. A survey on cutting edge research of well blowout risk assessment as well as numerical simulation of wellbore are described in this chapter.

- **Chapter 3:** Experimental design procedure for comparing and validating the numerical model and risk assessment model are elaborately explained in this chapter. The experimental observation and key findings are also presented sequentially. Experimental design and observations for numerical and risk assessment model are incorporated as a part of two separate journal publications.

- **Chapter 4:** This chapter discusses the theoretical background and simulation procedure of computational fluid dynamics model (numerical simulation model). Modelling of risk assessment model is discussed exhaustively in this chapter. The sections for numerical model and risk assessment model in this chapter are integrated as a part of two distinct journal publications

- **Chapter 5:** The results of numerical simulations are compared with experimental observations in this chapter. Further detailed analysis of numerical simulation results are incorporated in addition. Experimental validation of risk assessment model and results of risk assessment model are elaborated in this chapter.

- **Chapter 6:** This chapter summarizes the outcome and impact of the work. Possible future studies as well as the practical implementation of this work are presented.in this chapter.

Chapter 2

2 Literature Review

2.1 Brief Explanation of Blowout and Causes:

Blowout is considered as the continuation of uncontrolled flow of hydrocarbon from a wellbore as the consequence of kick and is considered the most severe incident in oil and gas industry. Especially in deepwater drilling, the consequences of blowout can be devastating because of oil spills and environmental impacts. The largest oil spill was

Figure 2-1 Deepwater horizon blowout (image source: The Times Picayune (Greater New Orleans))

Around 3.5 million barrels of oil had spilled into the gulf because of the SEDCO 135F IXTOC-I blowout which was experienced in 1979. The failure of blowout preventer to cut

the thicker drill collar allowed the oil and gas to flow to the surface. Figure 2.1 exhibits the aftermath of deepwater horizon blowout. The blowout incident was responsible for 11 workers death and continuation of 87 days oil spill. According to the investigation report, a chain of events caused the devastating consequence. Poor cementing was the reason for influx into the wellbore. Failure of kick detection and blowout preventer caused the loss of well control which escalated the kick to blowout.

2.1.1 Mechanism of Kick:

Kick is an unwanted or uncontrolled flow of formation fluid into the wellbore. Figure 2.2 presents the offshore drilling rig (a) and enlarged view of wellbore on the right side (b). Fluctuation of drilling mud's pressure below or above a certain range causes the influx into the wellbore [1]. Drilling mud is aimed at controlling the bottom hole pressure (BHP) in wellbore. Bottom hole pressure is composed of several components such as hydrostatic head, frictional pressure due to pumping, swabbing and surging pressure. Hydrostatic head is determined from the height of drilling mud column. Frictional pressure is created because of the fluid pumping through the drill string. The effect of swabbing is initiated when drill string is pulled out of the wellbore. Swabbing creates negative pressure. On contrary, surging is a positive pressure gradient, which is initiated when drill string is run into the wellbore.

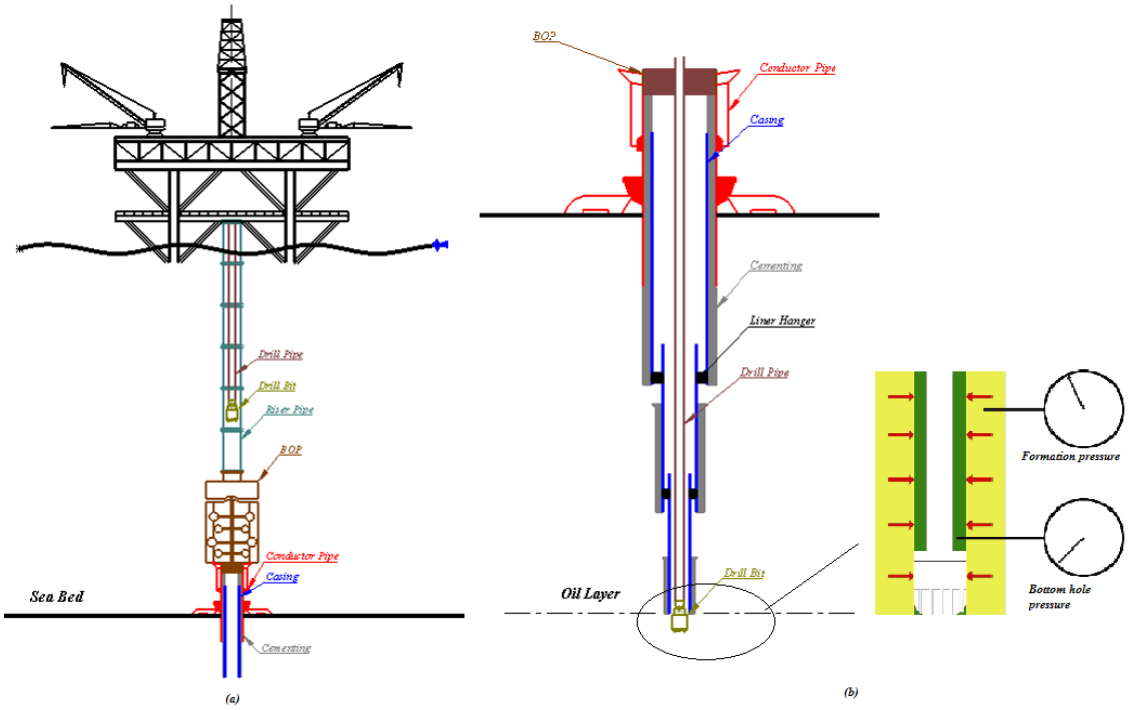

Figure 2-2 Offshore drilling rig and wellbore

To prevent the unwanted influx into the wellbore the bottom hole pressure is always maintained below the fracture pressure and above pore pressure. Pore pressure is the pressure exerted by the fluid inside pore of a rock. The BHP is greater than pore pressure to prevent the formation fluid to enter into the wellbore, which is known as overbalance situation. Pore pressure going above the BHP (underbalanced situation) initiates the influx into the wellbore. Loss circulation which is known as the flow of drilling fluid into the formation is observed when BHP is greater than fracture pressure [2]. Fracture pressure is the pressure that require to permanently deform the formation.

Following listed causes are considered as liable for the fluctuation of BHP as well as kick:

- Weight of drilling mud: To implement an optimum drilling mud program, controlling the mud weight is a major concern. Drilled solids can adversely affect the mud properties. Adding flocculants, dilution with water, installing solid particle removing equipment are few commonly used methods for controlling mud weight.

- Lost circulation: Continuation of drilling mud to flow from the wellbore to formation layer. Fractured formation or high permeability of formation layer causes the lost circulation.

- Tripping: Unable to maintain the wellbore pressure while tripping. Tripping is the act of drilling pipe pulling upward and running it back to the wellbore to change the drill bit or damaged drill pipe. Tripping consist of swabbing and surging.

    - Swabbing: The sudden decrease of downhole pressure due to the drilling pipe pulling upward is considered as swabbing [2]. The pressure fall can be too much to make the well underbalanced.

    - Surging: The increase of downhole pressure due to the drilling pipe pushing downward.

2.1.2 Kick Detection:

The escalation of kick into blowout depends on how quickly the mitigation measures or detection of kick are implemented. The well integrity is determined by continuous monitoring of drillstring torque, rate of penetration, volume of mud tanks, mud characteristics such as temperature and gas content. Rate of penetration is considered the

most noticeable drilling parameters to detect kick [3]. An increase in the rate of penetration indicates that the lower drilling margin has decreased due to the drop in BHP or rise in pore pressure. Similarly, irregular changes in the volume of drilling mud in mud tank and trip tank can be considered as a sign of kick. Decrease in the level of mud tank denotes the annular loss and increase in the volume of mud tank implies gas influx into the wellbore. A flow meter can be the most effective way to differentiate between the inflow rate and outflow rate of drilling mud. Besides those parameters, mud characteristics such as conductivity and density can be taken into account to detect kick. Furthermore, use of smart drilling pipe for direct monitoring of bottom hole pressure is the advanced way to detect early kick.

2.1.3 Well Control Operations

Well control can be defined as the methods which are used to maintain the control of well during an influx or kick in wellbore. Typical method of stopping a kick is well shut in. Hard shut in and soft shut in are two methods that are implemented during well shut in. Soft shut in refers to stopping the pump, open well control choke, close blowout preventer and close the well control choke. Alternately, hard shut in is closing the blowout preventer on closed well control choke. The main purpose of well shut in is to raise bottom hole pressure above pore pressure so that influx into the wellbore stops. The procedure of circulating out the kick or influx from wellbore is continued once kick is stopped [4].

Constant bottom hole pressure technique is implemented either by the one circulation method or the two circulation method to control a well. In the one circulation method the

shut in drill pipe pressure is recorded at first. Necessary mud weight to balance the formation pressure is measured, prepared and pumped into the wellbore. The casing pressure is maintained at shut in pressure by adjusting the well control choke. The mud is weighted to kill density and pumped through the annulus simultaneously in one circulation method. In the two circulation method, casing pressure is maintained at shut in pressure by bringing the pump in desired flow rate at first circulation. Influx being displaced, weight of mud is increased in second circulation to kill the well [5].

2.2 State of the Art of Numerical Simulation of Wellbore

A kick is considered to be an initiating event of blowout consequences. Formation pressure exceeding wellbore pressure is one of the most dominant reasons for an influx or kick into the wellbore. Use of heavy drilling fluid to over pressurize can increase the risk of fracturing the formation which results in lost circulation. Maintaining the wellbore pressure in a subsurface environment is not only challenging but also crucial in order to narrow the pressure margin. The situation becomes more perilous when the formation fluid contain gas [6]. Gas tends to expand while rising through the annulus causing significant variations in wellbore pressure. Furthermore, the rising speed of a gas kick increases as it expands and flows upward [7]. Due to the compressed volumetric behaviour of gas at the downhole, detection of a gas kick is cumbersome using the conventional approach of kick indicators (e.g. increase in flow rate out of annulus, increase in pit gain volume and abrupt increase in drilling rate). Ability to investigate the hydrodynamic behaviour of drilling fluid

as well as pore pressure at the downhole during a gas kick can provide significant improvement in well control techniques. An uncontrolled gas kick can lead to hazardous consequences: loss of life, damage to the environment and financial loss. The minimization of devastating consequences of a blowout is possible using appropriate well control mechanisms. A significant improvement can be achieved in quick response to a gas kick with appropriate well control techniques, when an exhaustive analysis of pressure, volumetric expansion and rising speed of a gas kick is available at the downhole.

Due to the safety issues in well design and well control, investigation using mathematical kick simulation was started four decades earlier. The first mathematical model proposed in 1968, assumed no pressure loss in the annulus and did not consider slippage speed between the drilling fluid and gas [8]. Further advancement in the mathematical modelling of a kick was achieved when it was incorporated with mass balance and momentum equations [9]. Empirical correlation between the gas speed and average speed of the mixture, restricted the realistic application of this model [10]. The evolution of kick simulation was continued by numerous researchers [11-15] who considered physical issues such as varied annulus geometry, two phase flow pattern, slip velocities between phases and gas solubility in drilling fluid [16].

To solve the transient two phase flow of liquid and gas in the wellbore, a finite difference formulation was adopted by Avelar [16]. Comparison of simulated and measured results was done by coupling the pressure loss computation and two-phase flow slippage [16]. A FORTRAN based one dimensional numerical code was proposed considering mass and momentum to study the blowing out process of a vertical wellbore [17]. Improvement of

one dimensional numerical method was achieved when compressed Navier-Stokes equations were solved incorporating numerous boundary conditions [18]. To reduce the numerical complexity of the two phase flow, a reduced drift flux model was proposed [19]. The drift flux method is also known as the mixture model, where a mixture of continuous and dispersed phases acts as a single fluid [20].

A detailed three dimensional transient visualization and numerical modeling, as well as experimental validation of a gas kick (stratified flow) using a turbulence model, multiphase flow model and compressibility is still pending. Though CFD is computationally expensive, it is quite capable of realistic simulation of a compressible multiphase flow. To simulate the multiphase gas-liquid compressible flow during a kick, commercial CFD package ANSYS FLUENT-15 is used, where governing equations of fluid dynamics such as continuity, momentum and energy equations are solved. Besides these governing equations, the standard pressure based algorithm is extended to Euler-Euler Volume of Fluid (VOF) transport equations for capturing the moving surfaces between the fluid phases. For turbulence modelling, Reynolds-averaged Navier-Stokes : Transition SST is used which combines the k- epsilon and k-omega model. The simulation model is simplified by considering air as an ideal gas for a compressible flow.

2.3 Evolution of Risk Assessment Model for Blowout Consequences:

Interpretation and breakdown of blowout accidents using a single failure are nearly impossible since these events are the outcome of a complex interaction of different failures

[32]. Numerous safety analysis methods have been proposed in the last 40 years for systematic and logical breakdown of complex multivariate processes [33]. In process system analysis, the qualitative and quantitative assessments of blowout risk are significant for maintaining the level of acceptable risk below the tolerance limit. Various blowout risk assessment methodologies have been reported in literature; for instance, fault tree analysis of a blowout starting from the causes of kick to the consequences [34] and a bowtie approach based on the case study of the Deep-water Horizon [35]. To overcome the circumscriptions of common causes of failure, Bayesian network approaches for quantitative analysis and through decomposition of blowout consequences have been thoroughly investigated [36], [37] and [38]. A barrier-based Swiss cheese method was proposed considering three level well controls. An additional barrier was established between reservoirs to prevent blowout events including the primary and secondary well control method [39].

The use of statistical and historical data often restricts the acceptability of blowout risk assessment methodologies [38], [40]. Due to the wide diversity of local parameters like weather conditions, formation pressure, temperature and porosity, the credibility of statistical data is always in question [36]. To overcome the challenge of unambiguous set of statistical data for specific types of wells and operating conditions, attempts have already been made, such as the SINTEFF database of enormous fields in study groups [41]. One of the major shortcomings of the SINTEFF database is not having any data for control systems and their reliability [42]. Significant strengthening of decision-making was achieved by developing a more realistic model based on the physical causal mechanism and extensive

use of expert evaluation, but this was characterized by the drawback of uncertainty of expert opinion [43]. To reduce the uncertainty of expert judgment a new approach was proposed based on Fuzzy Fault Tree Analysis [44]. The proposed methodology overcomes the weakness of conventional ETA but precise reflection of true conditions may not be possible due to the nature of data used [44].

Furthermore, in the risk assessment models developed by multifarious authors, kick detection is considered one of the crucial parts for the evaluation of blowout risk [45], [51]. On the basis of research carried out by the Bureau of Safety and Environment Enforcement (BSEE), it has been reported that about 50% of loss of well control events can be minimized or obviated by kick detection. Kick detection has become one of the major concerns since the Deepwater Horizon blowout on April 20, 2010. According to the investigative report of the Deepwater Horizon blowout, the changes of mud flowrate and pressure resulting from a kick were observed while the mud flowed through the riser [46], [36]. The loss of 11 lives could have been avoided by accurate and unambiguous detection of kick before it flowed through the riser. However, kick detection using surface-based variables that are being used in current practice is still incomplete.

Traditional or conventional kick detection methodology is based on the top side measurement which includes the pit volume totalizer, trip tank, pump pressure, drill pipe or stand pipe pressure. Insufficient weight of mud, tripping, swabbing, and lost circulation cause the fluctuation of hydrostatic pressure, which leads to a kick [47]. Pit volume totalizer has been widely used for kick detection but further extension of this methodology is restricted because of the time lag. To detect a kick by PVT the drilling mud needs to flow

all the way to the down-hole and then to return to the pit through the riser, which initiates the time lag [48]. Further improvement can be achieved by introducing a highly accurate flow meter that employs the Coriolis effect for electromagnetic sensing. A quicker and more precise comparison of the inlet and outlet flow rate of mud is possible since flow rate is measured just after the mud exits the riser. The detection of kick before the mud flows through the riser is still incomplete when introducing the flow meter just past riser until it is accompanied by down-hole parameters monitoring. This thesis is aimed at monitoring down-hole pressure combined with density, electrical conductivity and mass flow rate for quantitative risk assessment.

2.4 Synopsis

To obtain an extensive insight about well control techniques the study of hydrodynamic property of drilling fluid in wellbore is inevitable. Numerous mathematical models have been developed and proposed by researchers to study the hydrodynamic property. A three dimensional analysis and visualization using turbulence model, multiphase model and compressibility is still pending, which motivates the current work. Furthermore, quantitative risk analysis is an effective way to maintain the blowout risk within acceptable limit. Though numerous models are available to quantify the risk but integration of an on time risk estimation of kick will add a new dimension. A new methodology of on time risk estimation is proposed in this work based on this inspiration.

Chapter 3

3 Experiment Design and Result Analysis

The drilling experiments are conducted at the facilities available in Drilling Technology Laboratory at Memorial University of Newfoundland.

3.1 Flow Diagram of Experimental Setup

The central part of the experimental setup is a pressure cell which is made of a steel structure (see Figure 3.1). Figure 3.2 depicts a detailed and planned flow diagram of the

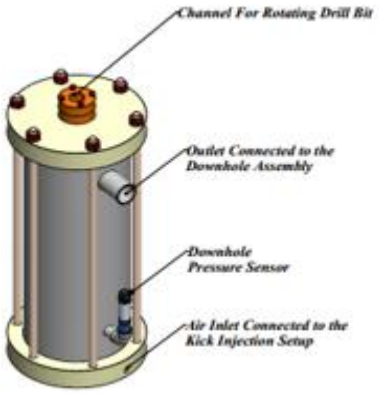

Figure 3-1 Pressure cell (see Figure 4-2 for detailed dimension)

experimental setup [30]. The pressure cell mimics a scaled down version of a wellbore. The fluid body of the pressure cell is considered as the computational domain for the numerical study. A detailed geometry of the computational domain corresponding to the pressure cell is presented in Figure 4.2. Synthetic rock rigidly fitted inside the pressure cell

can be drilled through a circular channel at the top of the pressure cell (see Figure 4.2). A positive displacement pump connected to a tank is used to move the drilling fluid through the drill string to the pressure cell. The drilling fluid mixed with cuttings is discharged through the outlet section. The downhole assembly consists of a pressure transducer, separator attached with a thermocouple, Coriolis flow meter and back pressure control valves. These valves can be adjusted manually to control the backpressure. A Coriolis flow meter and conductivity sensor, located at the very end of the assembly, are used to check the flow rate, density and electrical conductivity at the outlet. A pressure sensor connected at the bottom of the pressure cell monitors the pressure at the downhole. A small diameter hole at the bottom of the pressure cell is used to connect the air injection setup with the entire system. The check valve fitted in front of the hole at the bottom of the pressure cell prevents the drilling fluid from flowing into the air injection setup. An air compressor connected to an air tank acts as the source of air. A pressure regulator is used to control the air pressure flowing into the setup. A solenoid valve connected with a timer is used for closing the airflow to the setup. A gas flow meter, pressure transducer and thermocouple read the flow rate, pressure and temperature of airflow, respectively. Sensors are wired to the data acquisition system for continuous monitoring and recording (see Reference 57 for detailed overview)

3.2 Assumptions

The present study involves an experimental and numerical study of a kick in a wellbore. For simplification of the experimental work and to reduce the computational time of numerical simulation, the following assumptions are made:

- Water is considered as drilling fluid.
- To simulate and study the gas kick behaviour, air is considered as a kick gas.
- To analyze the compressibility effect, air is considered as an ideal gas.
- To reduce the computational time involving moving mesh, rotation of the drill bit is not considered.
- No heat transfer is considered between liquid and gaseous phases.
- This experimental study is not conducted with the presence of cuttings in the drilling fluid; incorporating a third phase in simulation is computationally expensive.
- Leaking of fluid is not considered for numerical simulation as it is a minor issue.

.

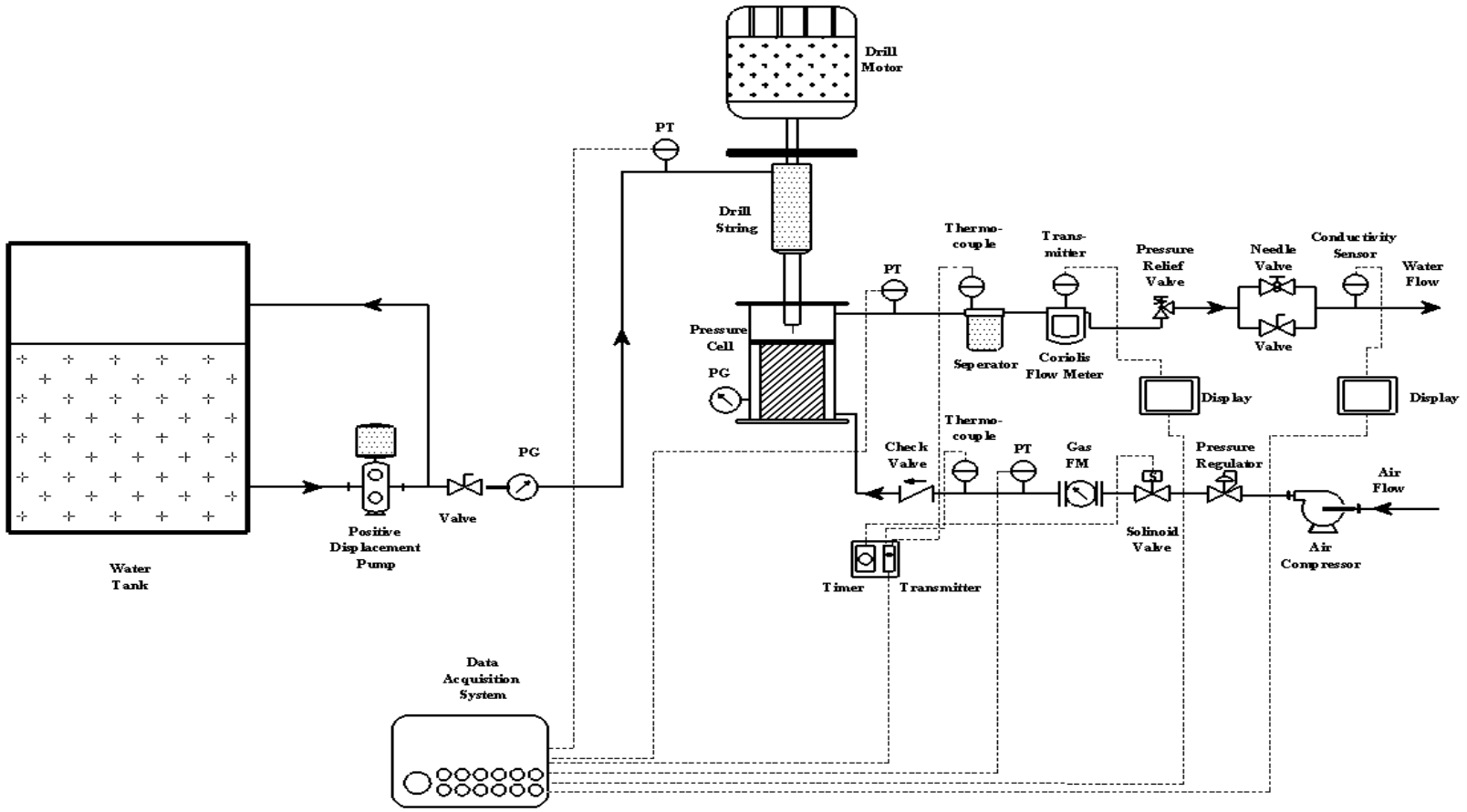

Figure 3-2 Flow diagram of experimental setup (see Reference 57 for detailed overview)

3.3 Experimental Procedure and Data Set for Numerical Simulation

Water is kept pumping at 3564 lb/hr from the storage tank at a constant rate through the drill bit as a drilling mud. To avoid the cuttings as a third phase in the numerical simulation, no synthetic rock is drilled while water is pumped from the storage tank. The drill string and drill bit are kept stationary during experimental study and during the artificial kick. Air

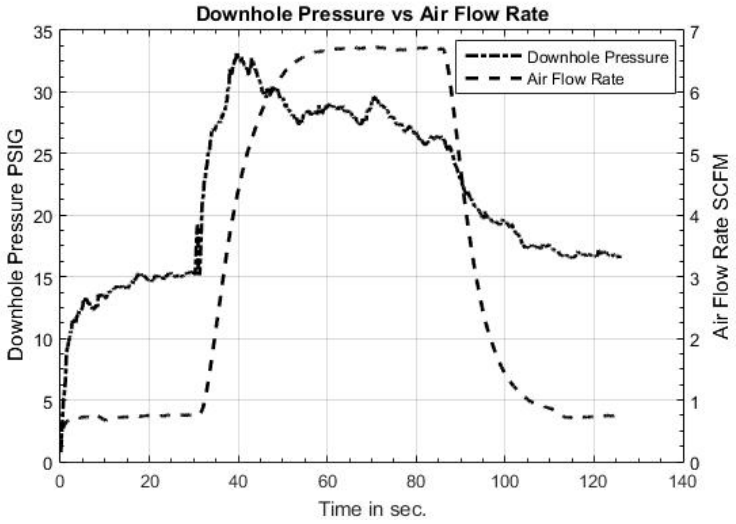

Figure 3-3 Change of downhole pressure with respect to kick

is used as a kick gas. An influx into the pressure cell is introduced by opening the solenoid valve for a certain period of time. The pressure sensor fitted at the bottom of the pressure cell reads the change in downhole pressure. Figure 3.3 depicts the change of downhole pressure while an artificial kick is introduced. The downhole pressure is 0 psi g at the very beginning of the experiment. The experiment is started from an empty pressure cell. The downhole pressure starts to increase as it fills up with water. After 20 seconds of run time,

the flow meter at the outlet is similar to the pumping rate. At 20 seconds, the downhole pressure becomes stabilized at almost 15 psi g. An intentional kick is introduced into the pressure at 30 seconds. Figure 3.3 depicts the increase of air flow rate as the solenoid valve opens. There is a leakage of air flow into the pressure cell before the solenoid valve is

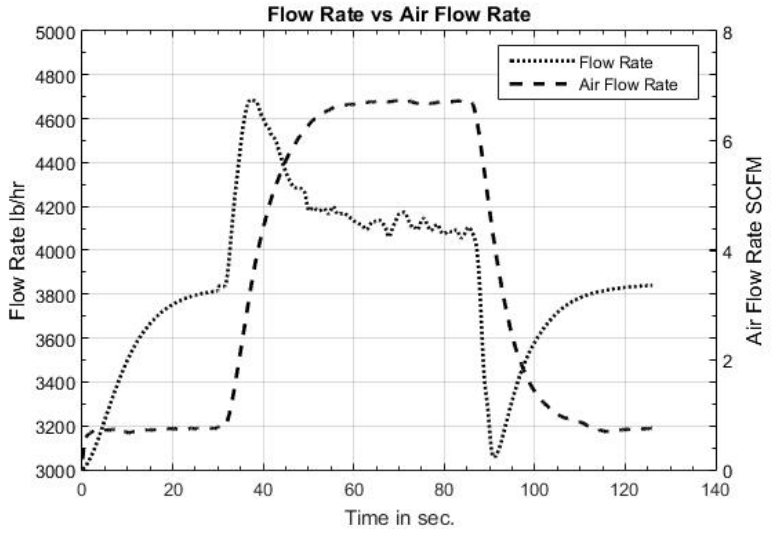

Figure 3-4 Change of mass flow rate at outlet during a kick.

opened. The leakage of air flow is considered as zero for this simulation purposes. The downhole pressure reaches the peak value at 40 seconds after the solenoid valve is opened. The mass flow rate at the outlet is measured by a Coriolis flow meter (see Figure 3.4). The change of outlet flow rate is significant while an artificial kick is introduced.

3.4 Experimental Procedure for Risk Assessment Model

To obtain the normal operating conditions or critical thresholds of parameters for flow condition, the experimental runs are piloted in two distinct steps. In the first step, experiment runs are conducted without any air influx to find the safe operational limits.

Three experimental runs are conducted at different pump flow rates to capture the varied operational range of downhole parameters.

- Experimental run 1: A window of total of 50 seconds of time is considered to obtain the normal operating condition of four downhole parameters and the airflow rate. To study kick detection based on the fluctuation of flow rate, pressure, density and conductivity, the entire experiment is simplified by considering water as a drilling fluid. To imitate the real case drilling scenario, water is kept pumping at a constant flow rate from the tank through the drill string into the pressure cell. Downhole parameters and airflow rate are recorded while the pump flow rate is maintained at around 3580 lb/hr. (see Section 3.4.1)

- Experimental runs 2 & 3: Experimental run 1 is repeated twice considering the pump flow rate around 4652 lb/hr and 5597 lb/hr.

In the second step, the above-mentioned three runs of the experiment are conducted including an air influx for a predetermined period of time. Water pump flow rates are kept almost identical to the three experimental runs in the first step.

- Experimental run 4: To capture the transient state between single phase and multiphase a period of 161 seconds of time window is considered. The maximum air volume flow rate is 7 SCFM while pump flow rate is maintained at 3580 lb/hr. (see Section 3.4.1)

- Experimental run 5: Around 4 SCFM airflow rate is maintained for a time interval of 50 seconds. The total time window is 156 seconds while the pump flow rate is 4652 lb/hr.

- Experimental run 6: Air pressure regulator is controlled to maintain the airflow rate of around 2.7 SCFM while water at 5597 lb/hr is kept pumping. 162 seconds of time exposure is considered.

3.4.1 Analysis of Experimental Data

Experiments are conducted in two different steps using three distinct flow conditions (see Section .3.4.). In the first step, the entire experiment is conducted without air influx into the pressure cell. Recorded noisy downhole parameters and airflow rate are processed by the discrete Kalman filter method [62] for noise reduction. Figure 3.5 presents the detailed data set for downhole parameters in a normal operating condition. In Experimental run 1, under a normal operating condition, the mass flow rate at the outlet is 3580 lb/s, while the downhole pressure is approximately 10.85 psig. Density is around 60.75 lb/ft^3 and electrical conductivity is 106 µS/cm. Normal operating conditions of downhole parameters and airflow rate for three diverse runs of the experiments are presented in Table 3.1. Mass flow rate at the outlet (see Figure 3.5 Mass flow rate) is almost identical to the water pump flow rate for Experimental runs 1, 2 & 3, which indicates a normal operating condition.

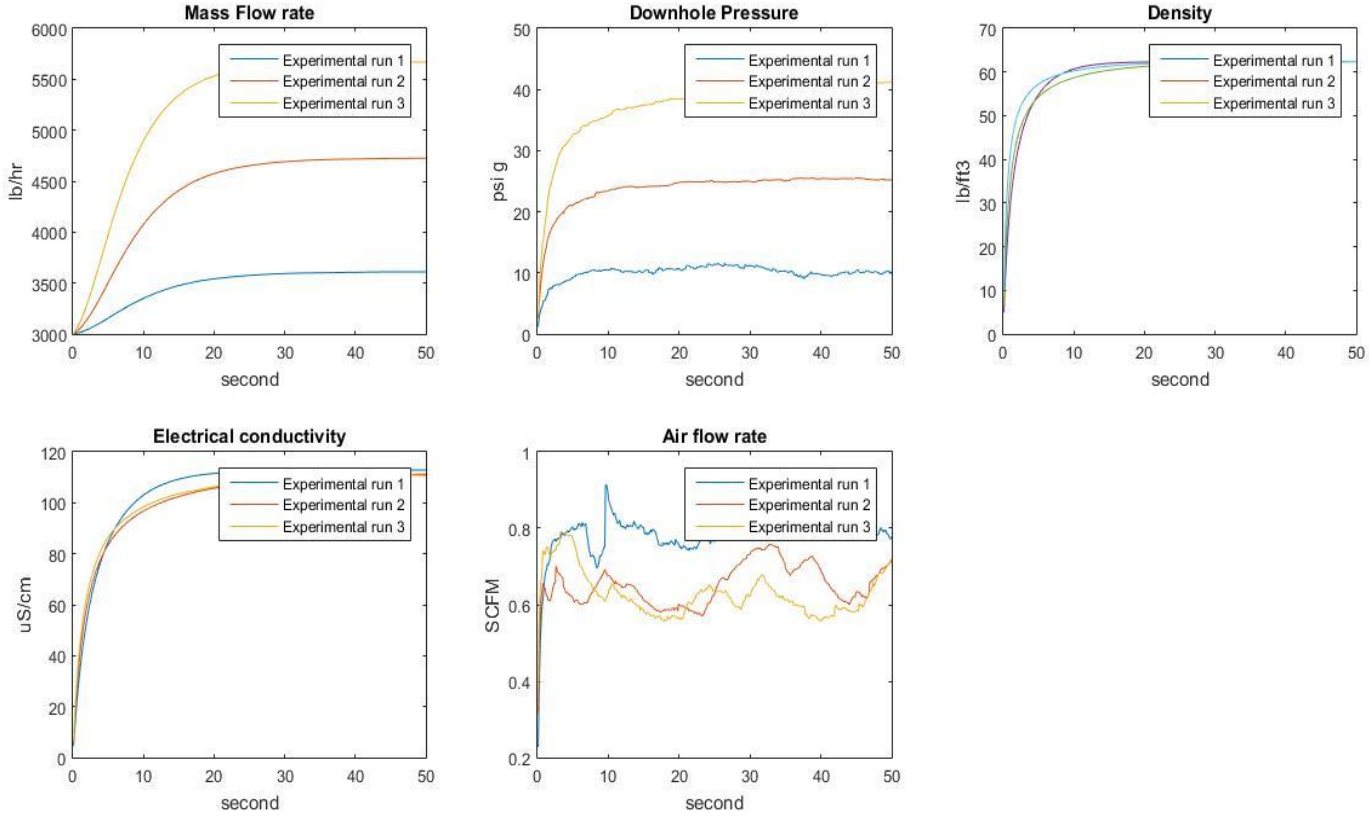

Figure 3-5 Downhole parameters and airflow rate under normal operating condition

Although, air is not injected into the pressure cell during the first step of the experiment, the airflow rate in Figure 3 5 delineates the amount of air leaking into the pressure cell. The corresponding values of air leaking into the pressure cell are considered critical threshold limits or normal operating conditions. The average values of air leaking into the pressure cell for Experimental runs 1, 2 and 3 are 0.80 SCFM, 0.67 SCFM, 0.65 SCFM respectively (see Table 3.1). In the second step, air is injected into the pressure cell for three experimental runs in Table 3.1. Fluctuations in downhole parameters and airflow rate are recorded and processed by the discrete Kalman filtration method [58]. Figure 3.6 depicts that the downhole parameters and airflow rate have diverged from a normal operating condition because of air influx into the pressure cell. To capture the transient stage between

Table 3-1 Normal Operating Condition of Primary Events

Index	Parameters/Primary events	Normal operating condition		
		Experimental run 1	Experimental run 2	Experimental run 3
1	Flow Rate	3580.00 lb/hr	4652.00 lb/hr	5597.00 lb/hr
2	Downhole pressure	10.85 psi g	25.13 psi g	40.07 psi g
3	Density	60.75 lb/ft^3	61.86 lb/ft^3	62.13 lb/ft^3
4	Electrical conductivity	106.00 uS/cm	108.00 uS/cm	108.00 uS/cm
5	Airflow rate	0.80 SCFM	0.67 SCFM	0.65 SCFM

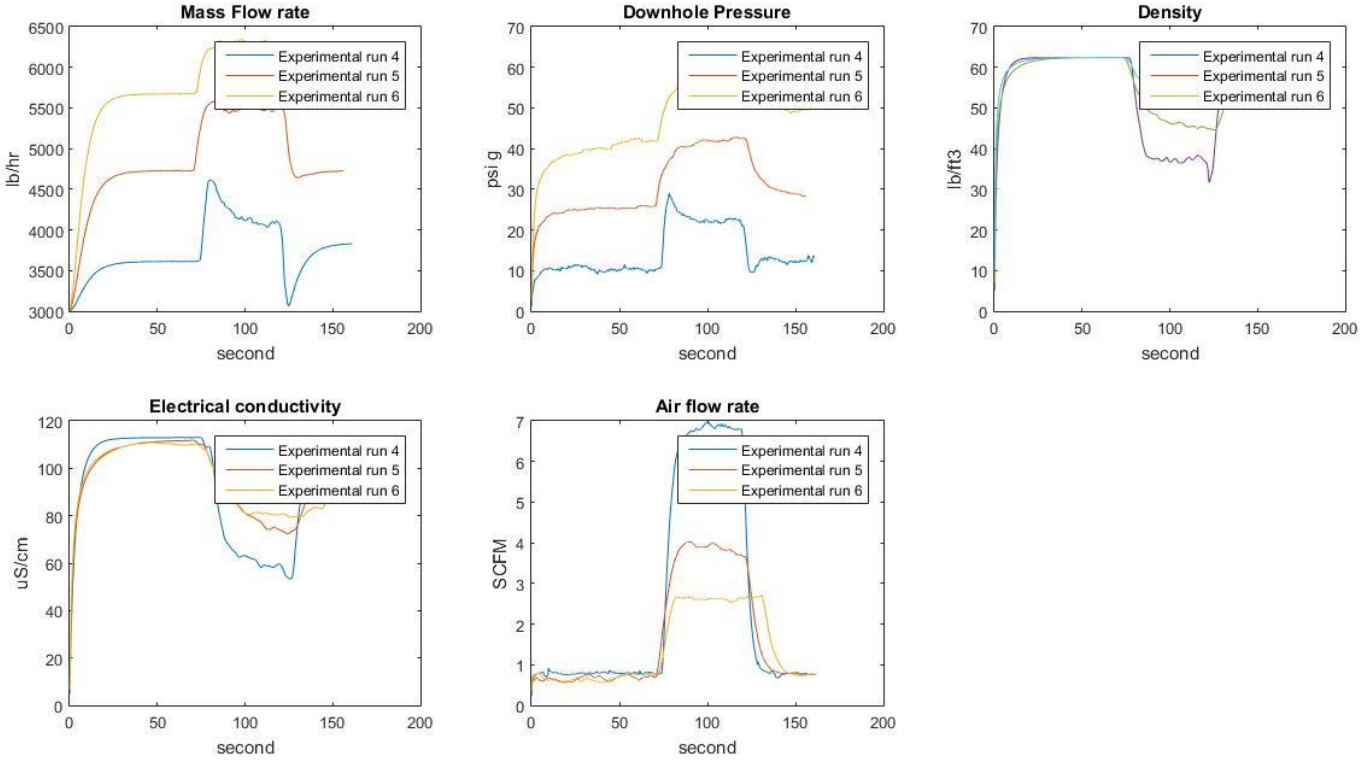

Figure 3-6 Downhole parameters and airflow rate while air influx into the pressure cell is introduced

the single phase and multiphase, the time window for the second step is maintained at least 150 seconds for each set of the experiment. Air influx is initiated approximately at 70 seconds and terminated at 120 seconds for each set of the experiment. Airflow rate shown in Figure 3.6 describes the three non-identical airflow rates for each experimental run. Analogous changes are observed for the mass flow rate at the outlet and for the downhole pressure, density and electrical conductivity simultaneously.

3.5 Synopsis

Experimental design and results for numerical simulation (CFD) and risk analysis are based on the same experimental setup. Experiments are conducted separately for numerical simulation and risk analysis part. In order to simplify the experimental design few assumptions are considered. To obtain the safe operational limit for risk assessment, experiments are conducted in two separate step. At first step, experiment was conducted without having a kick and in second step air is injected into the pressure cell to mimic a gas kick. To study the repeatability, three experimental runs are conducted with three discrete pump flow rates.

Chapter 4

4 Theoretical Model for Numerical Simulation and Risk Assessment

4.1 Theoretical Framework to Develop Dynamic Numerical Model

Viscous properties of fluid flow can be derived by solving the continuity equations of momentum and mass, known as Navier-Stokes (NS) equations. NS equations are capable of defining the turbulent properties of fluid whereas extensive computational cost needs to be considered for analytical solutions. To consider the effect of turbulence with reduced computational cost, time averaging of NS equations is performed, known as Reynolds Averaged Navier-Stokes (RANS) equations [21]. Computational fluid dynamics methods are used to solve RANS equations where the standard finite volume method (FVM) is applied to discretize the computational domain. Non-linear algebraic conservation and transport equations are linearized by discretization. Grid generation or meshing creates the finite volume method to solve the linearized equations [22]. The present study incorporates ICEM CFD as a meshing tool and commercial CFD package ANSYS FLUENT-15 for the numerical solution

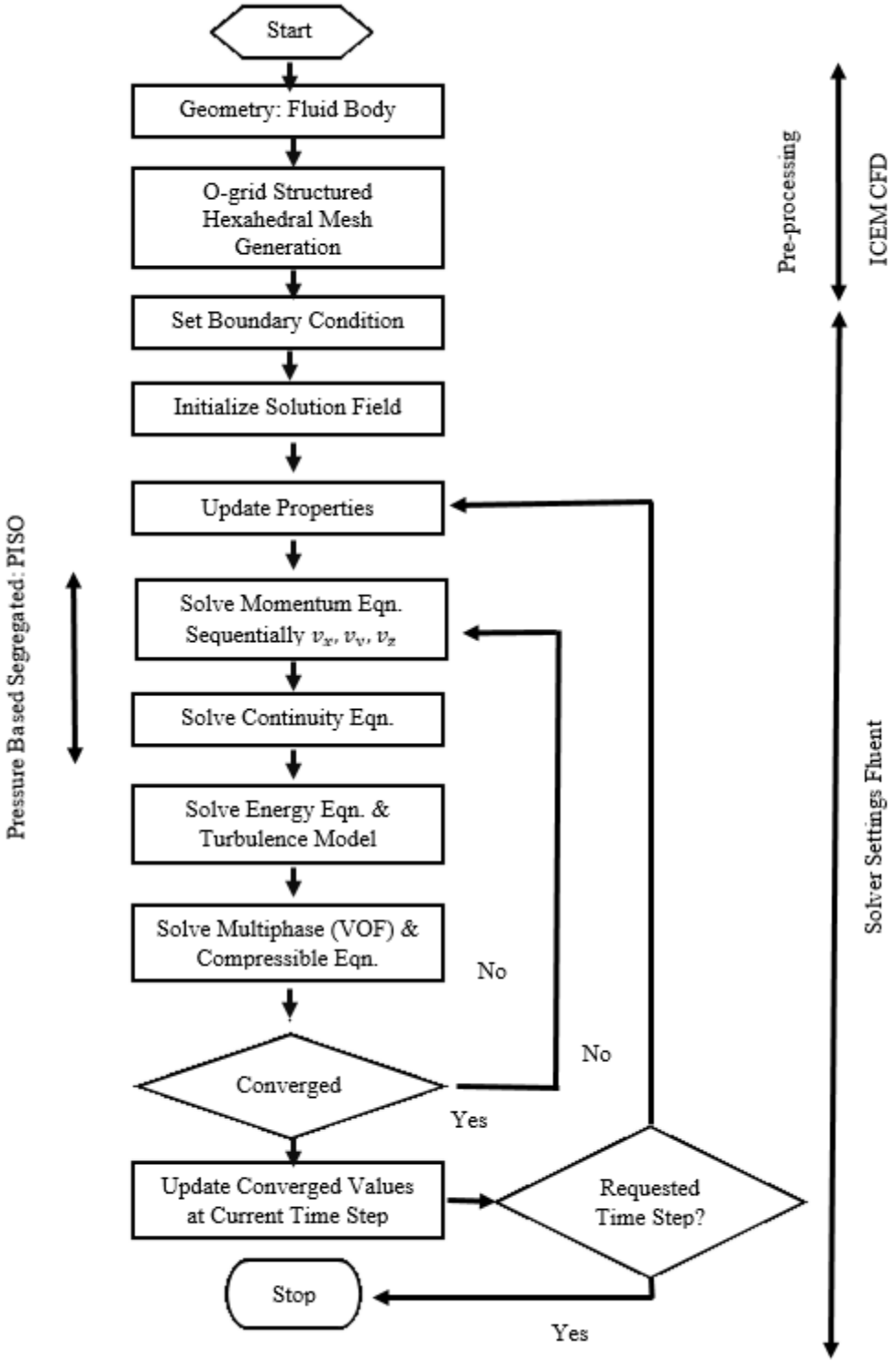

Figure 4-1 Framework of numerical simulation (transient state

4.1.1 Governing Equations

The governing conservation equations for unsteady, compressible flow are given by the following equations [23], [24], [25]. (See Appendix A for the scalar form of equation)

Equation of conservation of mass:

$$\frac{\partial \rho}{\partial t} + \nabla . \rho \vec{v} = 0 \tag{1}$$

where, ρ is the density and $\vec{v}$ is velocity vector of three dimension.

Conservation of momentum:

$$\frac{\partial (\rho \vec{v})}{\partial t} + \nabla . (\rho \vec{v} \vec{v}) = -\nabla p + \nabla . (\bar{\bar{\tau}}) + \rho \vec{g} + \vec{F} \tag{2}$$

$$\bar{\bar{\tau}} = \mu \left[(\nabla \vec{v} + \nabla \vec{v}^T) - \frac{2}{3} \nabla . \vec{v} I \right] \tag{3}$$

where p is the static pressure, $\bar{\bar{\tau}}$ is the stress tensor, and $\rho \vec{g}$ and $\vec{F}$ are the gravitational body forces in a vertical direction and the sum of external body forces. μ represents the dynamic viscosity and I is the unit tensor.

Energy equation:

$$\frac{\partial (\rho E)}{\partial t} + \nabla . [\vec{v}(\rho E + p)] = \nabla . \left[k_{eff} \nabla T - \sum_j h_j \overrightarrow{J_j} + \left(\bar{\bar{\tau}}_{eff} . \vec{v} \right) \right] + S_h \tag{4}$$

$$E = h - \frac{p}{\rho} + \frac{v^2}{2} \tag{5}$$

where E is the total energy, k_{eff} is the effective conductivity and S_h is the source term which is neglected as there is no reaction.

4.1.2 Turbulence Model

Time averaging NS equations, which are also known as RANS, are associated with an additional Reynolds stress term. Numerous turbulence models are available for modelling the mean quantities of Reynolds stress [26]. The $k-\epsilon$ and $k-\omega$ are two commonly used turbulence models based on Boussinesq approximations. Transition SST based on SST $k-\omega$ and two other transport equations are comparatively accurate for turbulence modelling [21], [27]. Additional transport equations represent the intermittency and transition onset criteria in terms of the momentum-thickness Reynolds number [28], [23]. The intermittency equation is formulated as follows:

$$\frac{\partial(\rho\gamma)}{\partial t}+\frac{\partial(\rho U_j\gamma)}{\partial x_j}=P_{\gamma1}-E_{\gamma1}+P_{\gamma2}-E_{\gamma2}+\frac{\partial}{\partial x_j}\left[\left(\mu+\frac{\mu_t}{\sigma_t}\right)\frac{\partial\gamma}{\partial x_j}\right] \quad (6)$$

The transition source is defined as:

$$P_{\gamma1}=F_{length}\rho S[\gamma F_{onset}]^{C_{a1}} \quad (7)$$

$$E_{\gamma1}=C_{e1}P_{\gamma1}\gamma \quad (8)$$

The destruction / relaminarization sources are defined as follows:

$$P_{\gamma2}=C_{a2}\rho\Omega\gamma F_{turb} \quad (9)$$

$$E_{\gamma2}=C_{e2}P_{\gamma2}\gamma \quad (10)$$

where Ω is the vorticity magnitude and S is the strain rate magnitude. F_{turb} is used to disable the destruction/ relaminarization sources.

4.1.3 Multiphase Model

The present study incorporates the volume of fraction (VOF) model for the multiphase model. VOF model solves two immiscible fluids by solving a single set of momentum equations and tracking the volume fraction of each fluid throughout the domain. The VOF formulation relies on the fact that these two fluids are not interpenetrating [23]. The flow properties ρ and μ are computed by the sum of partial densities and viscosities of liquid (l) and gas (g) [29].

$$\rho = \alpha\rho_g + (1-\alpha)\rho_l \tag{11}$$

$$\mu = \alpha\mu_g + (1-\alpha)\rho_l \tag{12}$$

where α denotes the liquid gas volume fraction

$$\alpha = \frac{V_g}{V_g + V_l} \tag{13}$$

The vapour volume fraction is computed by additional transport equations for the q phase as follows:

$$\frac{\partial \alpha_q}{\partial t} + \nabla.\left(\alpha_q v_q\right) = S_{cav} \tag{14}$$

S_{cav} represents the mass transfer between two phases which is considered zero for this study as there is no reaction or phase transfer.

4.1.4 Compressible Flow

Standard continuity and momentum equations describe the compressible flow and solving the energy equation correctly incorporates the coupling between the flow velocity

and temperature. For compressible flow air is considered as ideal gas for the present study. Ideal gas law can be written as follows [23]:

$$\rho = \frac{p_{op} + p}{\frac{R}{m_w} T} \tag{15}$$

where p_{op} is the operating pressure and p is the local static pressure relative to the operating pressure.

4.2 CFD Simulation Procedure

4.2.1 Steps of CFD Simulation

Numerical simulation of the 130 seconds of experimental work is computationally time consuming (see Figures 3.3 and 3.4). Considering the computational expense, the CFD simulation work is performed for a specific period of time in two steps. In the first 30 seconds of the time period of the experimental work, air is not injected into the pressure cell. In Figure 3.3, a small amount (0.73 SCFM) of air leakage is observed while the solenoid valve is closed. The leakage of air into the pressure cell is neglected and the first 30 seconds of experimental work are considered as a single phase flow for simulation work. The downhole pressure reaches peak value at 40 seconds which is 10 seconds after the starting of an artificial kick into the pressure cell (see Figure 3.3). Because the downhole pressure reaches the peak value at 40 seconds, the first 40 seconds of experimental work is selected for numerical simulation. The first 30 seconds of the experimental work is simulated as a steady state single phase flow, neglecting the air leakage into the pressure cell (see Figure 4.4 (a)). Simulation of 30-40 seconds of the experimental time window is

continued as a transient state two phase flow to capture the hydrodynamic behaviour of the air water mixture. The converged steady state simulation is continued as transient state.

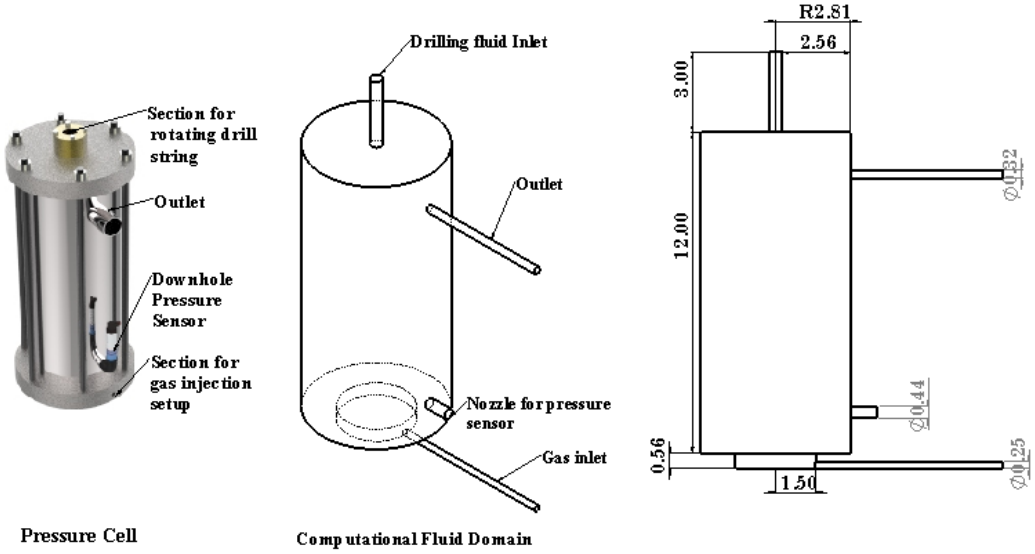

Figure 4-2 Pressure cell and dimension of computational domain in inches

4.2.2 Computational Fluid Domain and Meshing

Numerical simulation is performed considering the fluid domain inside the pressure cell. The section at the top of pressure cell enables the drill string to flow the drilling fluid into the pressure cell (see Figure 4.2). Gas is injected into the pressure cell through the gas inlet section. The considered fluid domain is presented in Figure 4.2. The drilling fluid inlet section which is considered as the inlet of water into the pressure cell is 0.50 inches in diameter. The radius of the computational domain is 2.81 inches and 12 inches in length. A 0.44 inch diameter nozzle is attached at the lower part of the pressure cell where the pressure sensor is connected. A needle valve installed at the outlet of the pressure cell reduces the flow area through the outlet section. The diameter of the outlet section is

reduced to 0.32 inches while the experiment is conducted. The gas inlet section is 0.25 inches in diameter. O-grid structured hexahedral meshing of the computational domain is presented in Figure 4.3. Blocking of the computational domain is performed strategically to maintain the conformal mesh between the main body and the sections such as the gas inlet, nozzle, outlet and drilling fluid inlet (see Figure 4.3 (b)). Blocking subdivides the computational domain into a configuration of a central block surrounded by radial blocks and the central block creates the O-grid that passes through the entire domain (see Figure 4.3 (c))

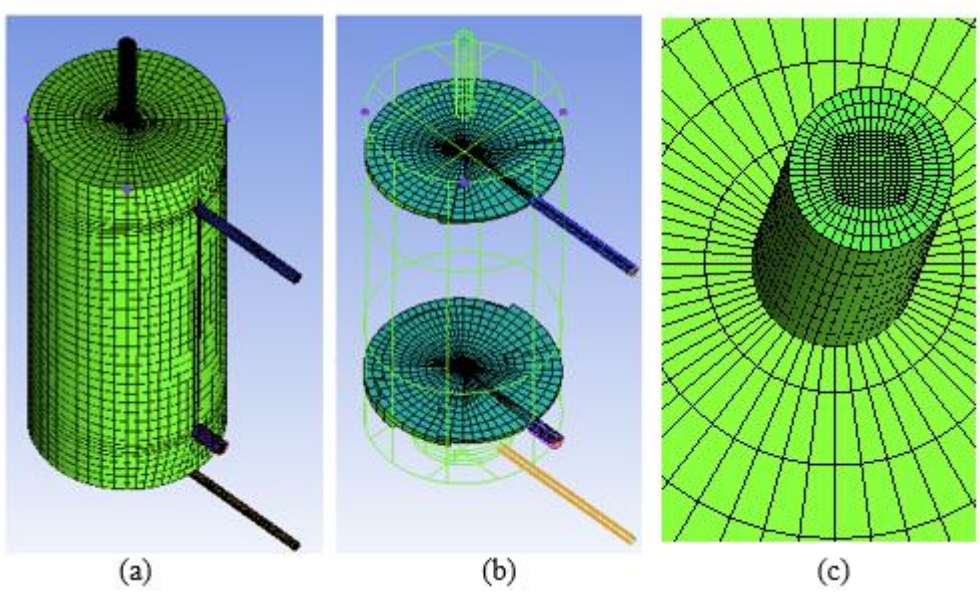

Figure 4-3 Structured hexahedral mesh of computational domain. (a) Isometric view. (b) Cut plane showing the conformal mesh. (c) Enlarged view showing the O-grid

4.2.3 Boundary Conditions

The steady and transient state part of the simulation is performed considering the mass flow rate of water at 0.99 lb/s (3564 lb/hr). As the leakage of air into the pressure cell is

neglected for the first 30 seconds of the experimental study, the mass flow rate of air into the pressure cell is considered zero for the steady state simulation (see Figure 4.4.a). The transient part of the simulation is continued for a 10 second time period which reflects the

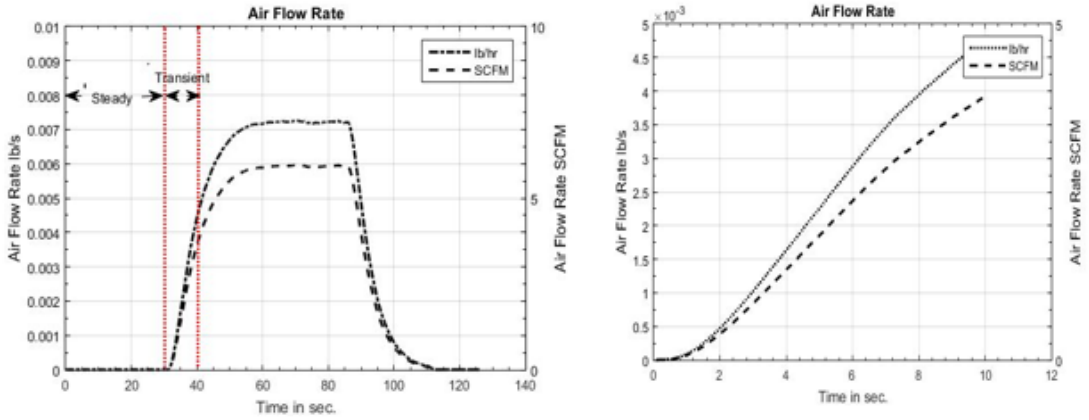

Figure 4-4 Air flow rate during experimental study. (a)(left) Air flow rate during steady and transient part of the simulation. (b) (right)Air flow rate in lb/s for the 10 seconds of the transient simulation

experimental study from 30-40 seconds test time (see Figure 4.4 (a)). To deal with the compressibility during simulation, air is assumed to follow the ideal gas law and it is selected as the primary phase. Water is selected as the secondary phase for simulation purposes. Figure 4.4.b depicts the enlarged view of air flow rate for 10 seconds of simulation time. The air mass flow rate is 0 lb/s at 30 seconds (0 seconds in Figure 4.4.b). At 10 second the air mass flow rate reaches to 4.8×10^{-3} lb/s. Air flow rate into the pressure cell is time dependent and increases with the increase of time (Figure 4.4 (b)). To define the time dependent boundary condition of air mass flow rate, a user defined function is written using the C programming language. Appendix B presents the user defined function (only the beginning logic) for the air mass flow rate [31]. Line 7 in Appendix B defines the logic of the air mass flow rate as zero

4.3 Blowout Risk Assessment Model

4.3.1 Bowtie Model

The bowtie model is considered one of the effective techniques of safety analysis of engineering systems. It enables the breakdown of the entire system, starting from the root causes and moving towards consequences. This model harmonizes the capabilities of the fault tree and event tree. The fault tree on the left hand side (see Figure 4.6) is an effective tool that proceeds deductively from the root causes to a top event (incident). The event tree on the right hand side (see Figure 4.6) depicts how failure of distinct safety barriers can lead to miscellaneous consequences. A typical bowtie model consists of basic events, intermediate events, top events, safety barriers and consequences. Though the bowtie model has many advantages, its use is limited in a complex system due to its limitation to model common cause failures and conditional dependencies [49]. Lack of a dynamic nature of this model also restricts the application of the bowtie model. The incapability of capturing evidence (new data) to update the probability of events is known as the static nature of the bowtie model [50]. A binary basic event in this model limits the further utilization of this model for a complex system. In this study, the bowtie model is used for graphical presentation and risk assessment of blowout consequences.

4.3.2 Evaluation of Blowout Phenomenon

Kick is considered an initiating event of a blowout where kick is termed as an influx into the wellbore above a certain amount. An influx in a wellbore is observed while drilling if

the bottom hole pressure (BHP) is not maintained within a specific boundary of pore pressure and fracture pressure. Figure 4.5 presents a typical drilling operation where BHP is maintained below the fracture pressure and above pore pressure [52]. BHP greater than pore pressure prevents the formation fluid from flowing into the wellbore. On the other hand, BHP less than fracture pressure prevents the pressure drop in the wellbore due to lost circulation or drilling fluid flowing into the formation. BHP can be calculated from three major parameters known as hydrostatic head, frictional pressure loss and surge/swab pressure [43].

$$BHP = BHP_{hydrst} + BHP_{fr.pl} + BHP_{srg/swp} \quad (16)$$

Considering Equation (42), the main causes of an influx into the wellbore (kick) can be identified by categorizing the entire drilling operation into three sub drilling operation, such as static BHP_{hydrst}, circulating $BHP_{fr.pl}$ and tripping $BHP_{srg/swp}$. The product of density and vertical length the of mud column help to estimate the hydrostatic head. Density and the mud column are strongly influenced by the dilution of mud and lost circulation respectively, which are considered crucial parameters leading to the fluctuation of BHP and then kick. Density of mud is also affected by the gas influx which basically escalates the kick. $BHP_{fr.pl}$ defines the frictional pressure loss as due to the drilling mud flowing through the drill string, and this is a direct function of drilling mud pump pressure. Swabbing occurs during the tripping operation, resulting in a reduction of BHP because of the drill string pulling upward. To the contrary, surging gives rise of BHP due to the drilling string moving downward.

Well control methods also known as well barriers [52] are initiated followed by a kick occurrence. According to NORSOK D-010 [53], well barriers are the amalgamation of one or multiple barriers dependent on each other based on the objective of preventing the uncontrolled flow of formation fluid through the well bore to the surface. Sequential classification of well control methods is done so that stepwise control operations can be carried out sequentially (see Section 4.3.3). Failure of sequential well barriers results in an uncontrolled flow of hydrocarbon from the formation layer to the drilling rig surfaces, escalating the chance of a catastrophic event, a blowout.

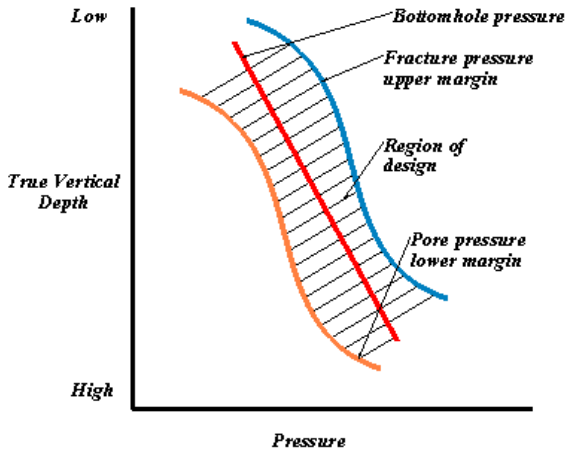

Figure 4-5 Typical scenario of BHP margin [52]

4.3.3 Key Indicator and Safety Barriers of Blowout

A kick in a wellbore is considered an initiating event in the blowout phenomenon, so the identification of parameters to detect kick is of utmost importance. Due to the time lag of the pit volume totalizer (PVT) to detect the kick [48], a Coriolis flow meter measuring the flow rate of drilling mud that is located right next to the riser is included. Density and

electrical conductivity of drilling mud are directly related to the influx in a wellbore. Downhole pressure is also taken into account for detection of kick. Based on these four parameters, an experimental setup established in Reference [57] is used in this study to simulate diversified flow conditions and monitor these four parameters. Safety barriers or well control barriers prevent the uncontrolled flow of formation fluid from the reservoir during kick. A barriers principle is followed in the UK and the US; the barriers are named the primary barrier and secondary barrier [39]. The hydrostatic head is referred to as the primary barrier, and topside equipment such as the BOP and the Christmas tree are considered secondary barriers [54]. Three level well control theory is a significant part of well control activities and blowout development stages [39]. The three phases of well control theory are primary well control, secondary well control and tertiary well control. The process carried out in the oil and gas industry to regain the well integrity and hydrostatic pressure between the pore pressure and fracture pressure after the occurrence of kick is defined as well control. The three level well control theory is more comprehensive compared to two-barrier principle.

Primary well control refers to the maintaining of hydrostatic pressure of the drilling mud column. Since hydrostatic pressure is the function of the density and pump pressure of drilling mud, drillers can use kick detection as a sign to adjust the density and pump pressure to regain the hydrostatic pressure within a predefined pressure boundary. The secondary well control method is carried out when the primary well control method fails to maintain the hydrostatic pressure. Secondary well control starts with an immediate well shut in by closing the pipe ram in the BOP and stopping the drilling mud pump. A typical

shut in procedure is known as a “soft shut in’’, where keeping the choke valve open at first, the pump is turned off and the BOP is closed, and then gradually the choke valve is closed [55]. To the contrary, closing the BOP and stopping the pump under the closed choke is known as a “hard shut in”. Upon successful completion of shut in, circulating the kick out from the well bore is done by the Drillers method or Engineers method. The Driller’s method consists of two circulations, named the first circulation and second circulation, while the Engineer’s method employs one circulation. Failure of the secondary well control method leads to the complete shutdown of the wellbore by disconnecting the drill pipe using a blind shear ram and closing the annulus by annular preventer. A severe incident could occur if the BOP fails to prevent the flow of unwanted influx to the surface. According to the three level well control theory, tertiary well control is a technology for recovering the control of a wellhead after the blowout [39]. Tertiary well control also refers to the partial or complete abandonment of a well. The barite plug and cement plug are two common features of tertiary well control. A cement plug involves pumping cement into the well but is associated with the risk of complete abandonment of a well. Barite plug is prepared by mixing a heavy slurry of barite in the water or diesel.

4.3.4 Modelling of Blowout Risk Analysis Using Bowtie

To investigate the envisaged blowout consequences, a graphical presentation of an exhaustive blowout scenario has been provided using a bowtie model in Figure 4.6. The bowtie approach of blowout risk analysis embraces the fault tree for kick detection and the event tree for safety barriers.

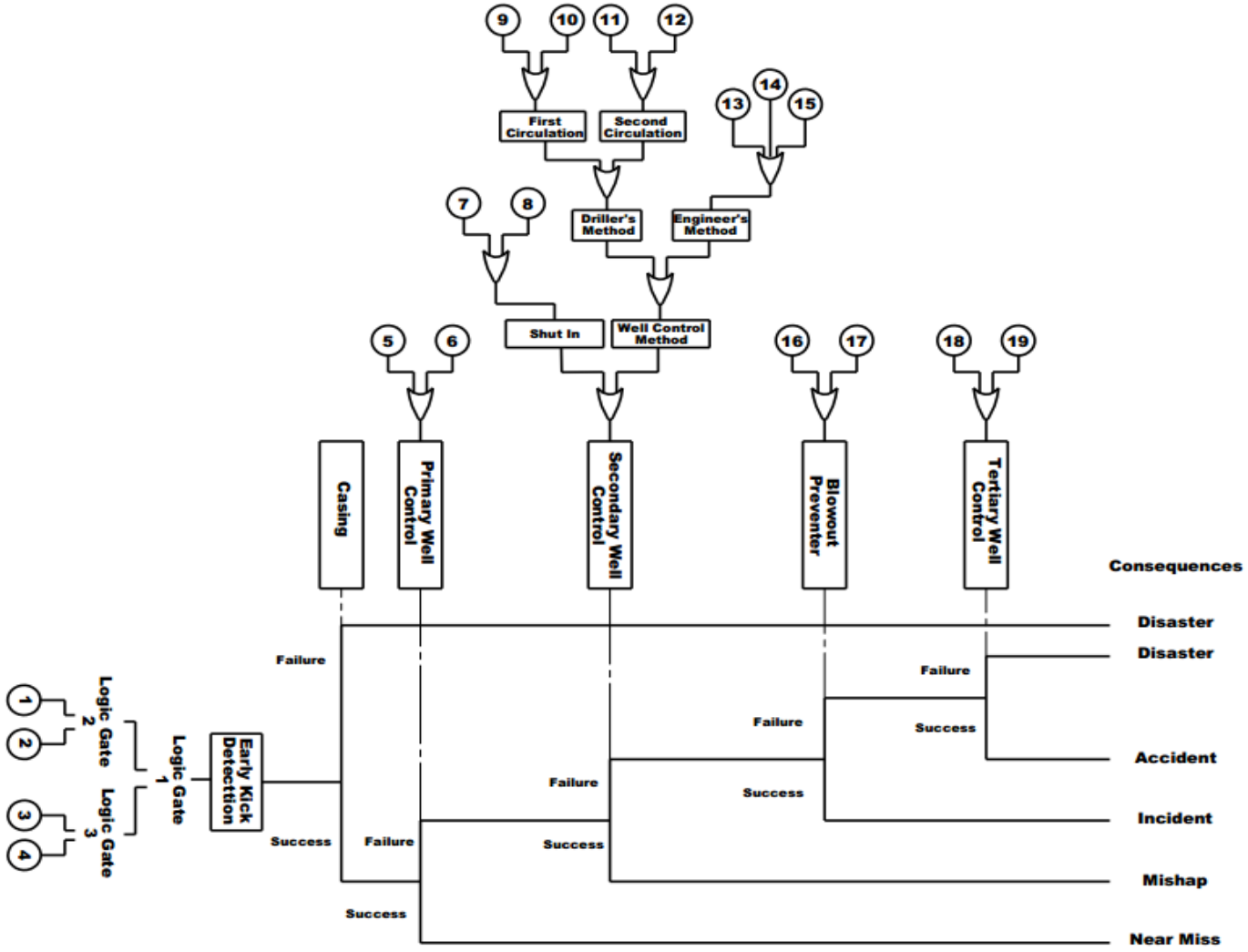

Figure 4-6 Bow Tie risk assessment model

4.3.4.1 Kick detection fault tree

Kick indicators described in Section 4.3.3 for detection of kick can be combined by using numerous structures of logical combinations. Figure 4.7 presents few possible structures of logical combinations for kick detection parameters. Structure 1 in Figure 4.7 is considered as a fault tree for modeling the bow tie risk assessment model As described in section 4.3.3, downhole parameters such as flow rate, pressure, electrical conductivity and density are used to enumerate the probability of kick. Selected downhole parameters are statistically independent and binary in nature. Different plausible scenarios can be envisaged by amalgamating primary events or downhole parameters through different non-identical logical combinations. Table 4.1 delineates the selected scenarios of logical combinations for selected the logical structure 1. The main purpose of studying numerous non-identical logical combinations is to improve the reliability of kick detection and also reduce the false alarms of kick detection. Appropriateness of selected logical combinations is tested through a known experimental kick testing setup (see Section 5.2.3).

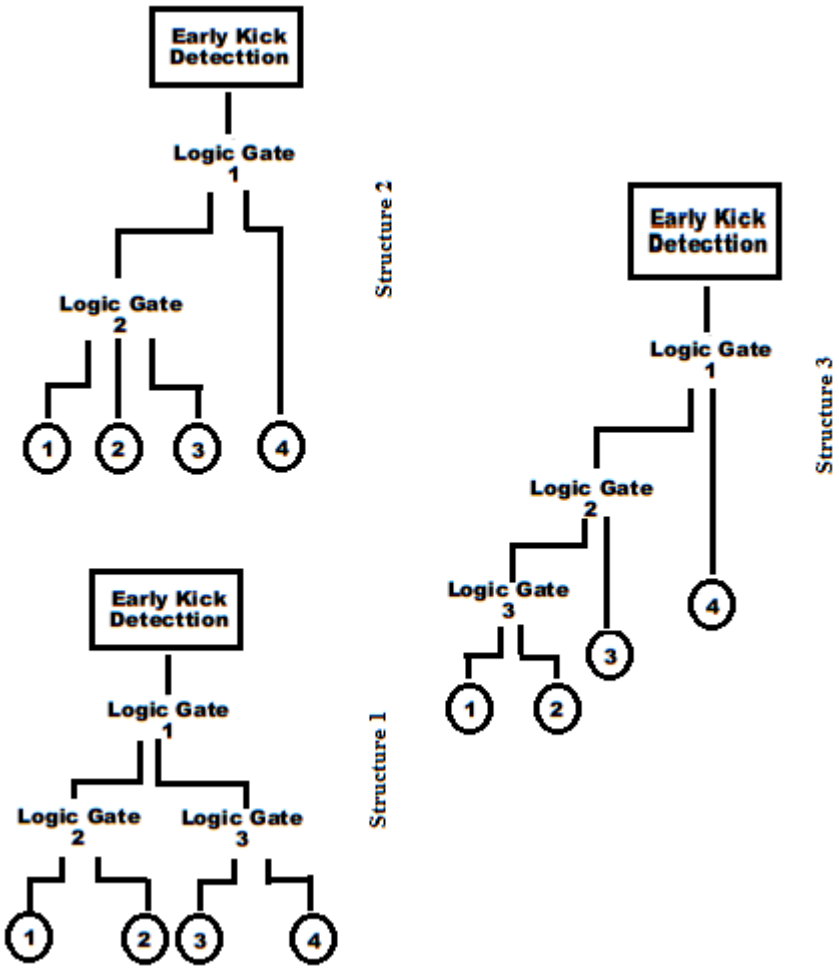

Figure 4-7 Kick detection fault tree

Table 4-1 Selected logical combinations for kick detection in Figure 4.7

Index	Primary events				Logic gates		
	1	2	3	4	1	2	3
1	Flow rate	Downhole Pressure	Density	Electrical Conductivity	OR	OR	OR
2	Flow rate	Downhole Pressure	Density	Electrical Conductivity	AND	AND	AND
3	Flow rate	Downhole Pressure	Density	Electrical Conductivity	AND	OR	OR
4	Flow rate	Downhole Pressure	Density	Electrical Conductivity	AND	OR	AND
5	Flow rate	Downhole Pressure	Density	Electrical Conductivity	AND	AND	OR
6	Flow rate	Downhole Pressure	Density	Electrical Conductivity	OR	AND	AND
7	Flow rate	Downhole Pressure	Density	Electrical Conductivity	OR	OR	AND
8	Flow rate	Downhole Pressure	Density	Electrical Conductivity	OR	AND	OR
9	Flow rate	Electrical Conductivity	Downhole Pressure	Density	AND	OR	OR
10	Flow rate	Electrical Conductivity	Downhole Pressure	Density	AND	OR	AND
11	Flow rate	Electrical Conductivity	Downhole Pressure	Density	AND	AND	OR
12	Flow rate	Electrical Conductivity	Downhole Pressure	Density	OR	AND	AND
13	Flow rate	Electrical Conductivity	Downhole Pressure	Density	OR	OR	AND
14	Flow rate	Electrical Conductivity	Downhole Pressure	Density	OR	AND	OR
15	Flow rate	Density	Downhole Pressure	Electrical Conductivity	AND	OR	OR
16	Flow rate	Density	Downhole Pressure	Electrical Conductivity	AND	OR	AND
17	Flow rate	Density	Downhole Pressure	Electrical Conductivity	AND	AND	OR
18	Flow rate	Density	Downhole Pressure	Electrical Conductivity	OR	AND	AND
19	Flow rate	Density	Downhole Pressure	Electrical Conductivity	OR	OR	AND
20	Flow rate	Density	Downhole Pressure	Electrical Conductivity	OR	AND	OR

4.3.4.2 Safety Barriers Event Tree

In addition to the fault tree for kick detection, an event tree (see Figure 4.6) including five safety barriers is considered in the bowtie risk analysis model. The consequences of the failure of independent safety barriers are classified according to the definition of abnormal events derived by Rathnayaka et al. [56]. Categorized consequences are presented in Table

Table 4-2 Category of blowout consequences

Index	Consequences	Description
1	Near Miss	Event that does not result in actual loss but has potential to do so.
2	Mishap	Event that causes minor health effects and/or minor effects to property and environment.
3	Incident	Event that can cause considerable harm or loss.
4	Accident	Event that may cause one or more fatalities or permanent major disabilities.
5	Disaster	Event that can cause multiple fatalities and extensive damage to the property, system and production.

4.2. Casing is considered to be an indispensable and primary safety barrier as the failure of casing governs the failure of holding a kick inside casing. Failure of casing leads to the consecutive failures of primary well control, secondary well control, BOP and tertiary well

control. The consequence of casing failure is classified as disaster in Figure 4.6. Disaster is also envisaged upon failure of secondary well control, BOP and tertiary well control followed by the success of casing. Success of casing and primary well control leads to the consequence of a near miss.

4.4 Synopsis

Reynolds Averaged Navier Stokes equations are solved for the numerical simulation of multiphase flow. A time averaging term which is known as the Reynolds Stress terms are associated with the solution of the Reynolds Averaged Navier Stokes equations. Numerous methods are available for modelling the Reynolds Stress term. The mean quantities of Reynolds stress are defined by the Transition SST $k-\omega$ turbulence model. Finite volume method is used for discretization. The numerical model incorporates the volume of fraction model for multiphase modeling. To quantify the blowout consequences, a risk assessment model is proposed based on the bowtie approach. Fault tree of the bow tie model is linked to the experimental setup where kick detection indicators are considered. Well control techniques are considered as safety barriers to model event tree of the bow tie risk assessment model.

Chapter 5

5 Results & Discussion

5.1 Analysis of CFD Simulation Results

5.1.1 Flow Pattern Analysis in Computational Fluid Domain

To analyze the flow pattern and the turbulence of the two phase flow, an exhaustive analysis of the air water volume fraction is performed. In Figure 5.1 (a), the time dependent air volume fraction is presented. A plane is considered at the middle of the computational domain capturing the outlet section and the inlet section of air and water. The blue contour describes the zero volume fraction of air; in other words, the blue contour exhibits the presence of water. The red contour represents the volume fraction of air 1. At t=1.25×10^{-2} seconds, the computational domain is filled with water, which is presented by the blue contour. A three dimensional illustration of air volume fraction is performed by volume rendering in Figure 5.1 (b). As the mass flow rate of air is zero at 1.25×10^{-2} seconds, the presence of air is not observed in Figure 5.1 (b) at t=1.25×10^{-2} seconds. The air mass flow rate through the gas inlet section is observed at t=1.20 seconds (see Figure 5.1 (b)). The air volume fraction in the computational domain increases as time passes, from t=1.20 seconds to t= 9.52 seconds. Air starts to accumulate at the top of the

pressure cell and at t=4.5 seconds air starts to flow through the outlet section. In Figure 5.1 (a), at t=4 seconds a straight blue streamline is observed from the inlet section of water, which exhibits the water flow through the drilling fluid inlet section of the computational domain. The streamline of water becomes clearly visible at t=7 and t=9.525 seconds

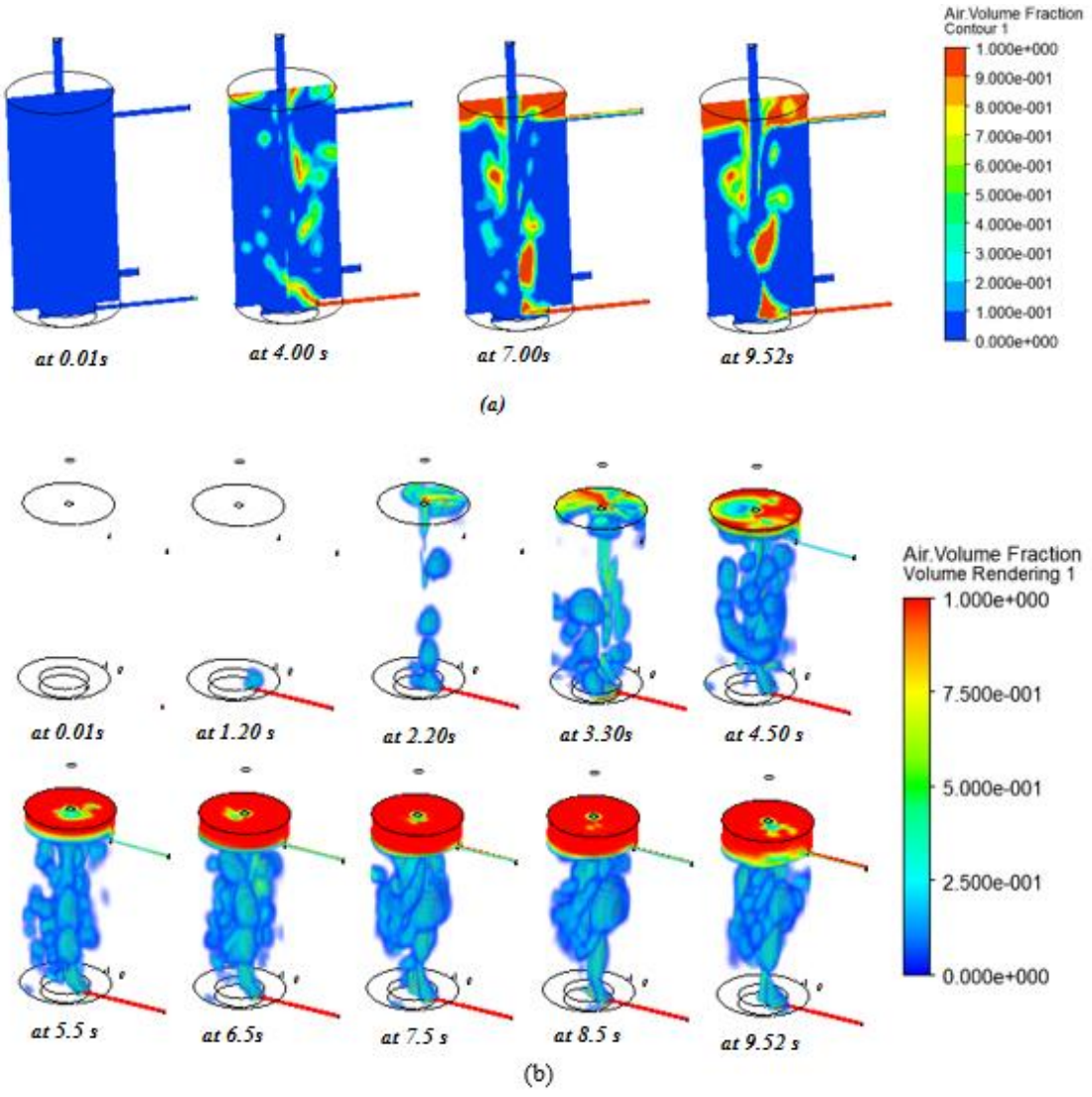

Figure 5-1 (a) Air water volume fraction at mid plane. (b) Volume rendering of air volume fraction

as the air starts to accumulate at the top of the pressure cell. Water flows through the middle of accumulated air at the top of the pressure cell. Furthermore, at the outlet section, air

flows through the upper portion of the pipe and water flows through the lower portion of pipe.

5.1.2 Validation of CFD simulation

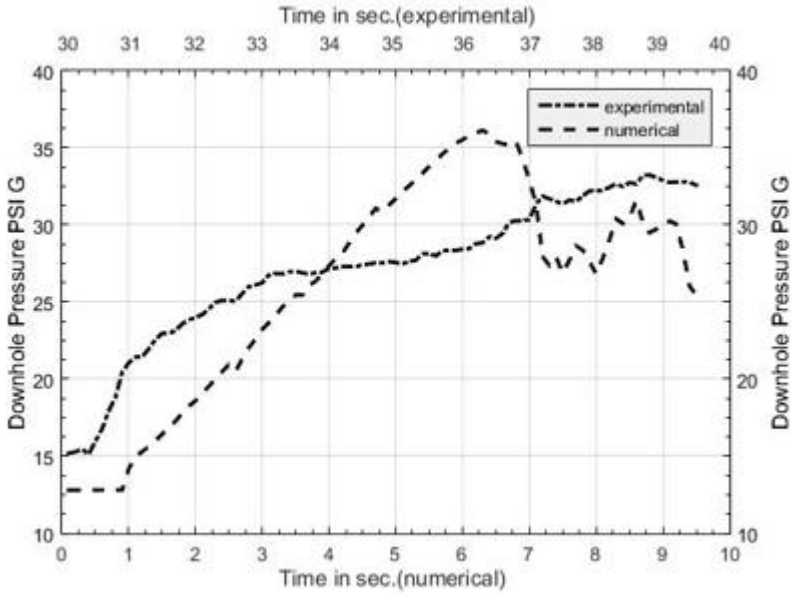

Figure 5-2 Comparison of numerical and experimental results

Numerical simulation results are compared with the experimental results in Figure 5.2. Downhole pressure recorded between the time periods of 30 to 40 seconds is compared with the 9.52 seconds of the simulation results. The first 30 seconds of experimental work are simulated as a steady state considering a single phase flow into the pressure cell. The converged steady state simulation is continued for 9.52 seconds as a transient state. The predicted downhole pressure by steady state simulation is 12.5 psi g. The downhole pressure observed before the influx into the pressure cell is 15 psi g (see Figure 3.3 and Figure 5.2). During the influx into the pressure cell, downhole pressure increases within

the time period of 30-40 seconds. Numerical simulation results also exhibit a similar trend to the experimentally observed result (Figure 5.2). In Figure 5.3, the percentage of error between the numerical and experimental results is plotted. At t=1 seconds, the maximum percentage of under prediction of downhole pressure is observed. The highest percentage of over prediction is observed at t=6 seconds. The percentage of error between the experimental and numerical results starts to decrease after 6 seconds of the simulation time. The flow pattern going into the pressure cell starts to stabilize after 6 seconds of simulation time. Similarly, in Figure 5-4 the difference between numerical and experimental result is presented. The maximum error between the experimental and numerical was observed at t=1 seconds. Likewise, in Figure 5-3 the Figure 5-4 represents the same trend which is the decrease in error when the flow gets stabilized. In Figure 5.1 (b), an analogous flow pattern of air and water into the pressure cell is observed at 6.5, 7.5, 8.5 and 9.5 seconds. Stabilizing the flow pattern in the pressure cell reduces the percentage of error between the numerical and experimental results. The percentage of error fluctuates 0 to 20 in the time period of 7 to 9 seconds, while the flow pattern in the pressure cell stabilizes.

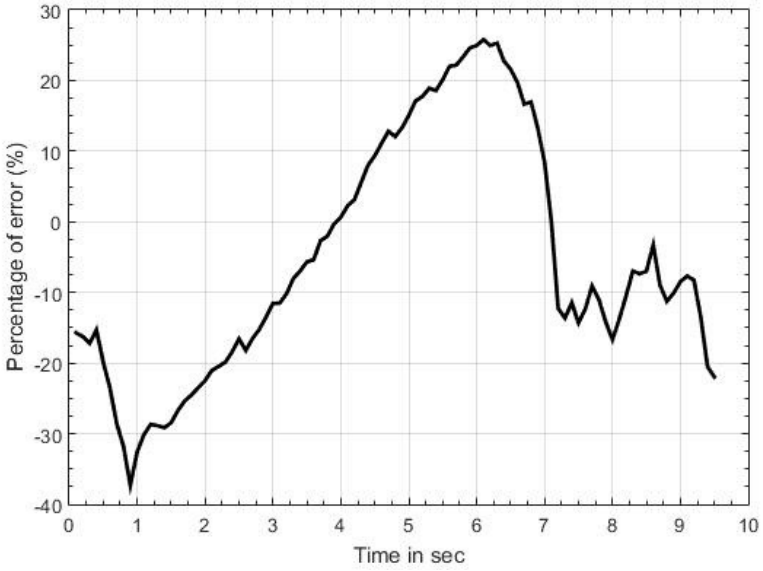

Figure 5-3 Percentage of error in numerical prediction

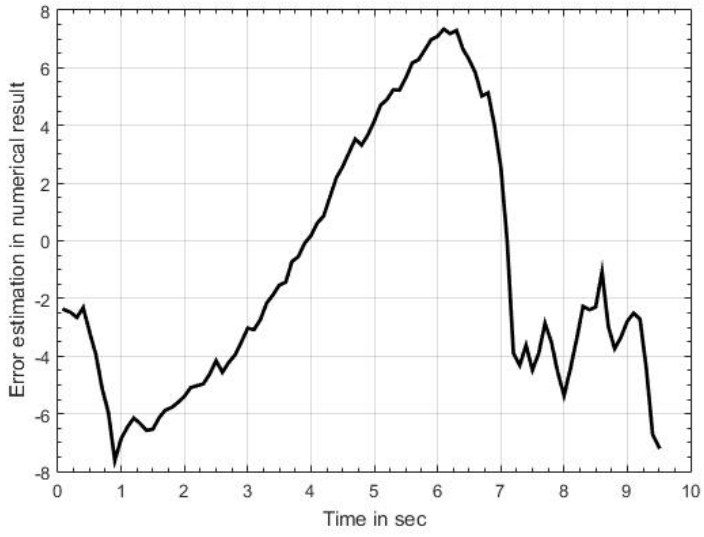

Figure 5-4 Error in numerical prediction and experimental result.

5.1.3 Velocity Profile Characteristics

The velocity volume rendering in Figure 5.4 exhibits the change in velocity gradient at the outlet pipe while an artificial kick is injected. At t=1.25×10^{-2} seconds, the contour at the outlet section describes the velocity of the water flow rate through the outlet pipe. The velocity of water flow rate is below 49 m/s before the influx of air. The velocity profile drastically changes while air is introduced into the pressure cell and flows through the outlet section. The maximum velocity of 197 m/s is observed at the tip of the outlet pipe when t= 9.52 seconds. The water and air are immiscible mixture and the gravitational force aids the air to flow through the upper portion of the outlet section (see Figure 5.1 (a)). The immiscible mixture of air and water flows at two different speeds through the outlet section. In Figure 5.4, the maximum velocity profile is observed for air flowing through the upper portion of the outlet section.

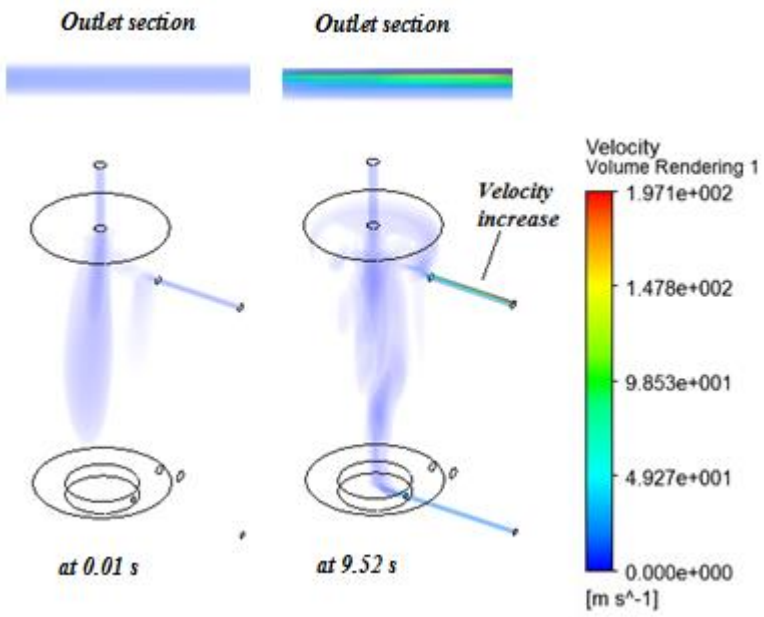

Figure 5-5 Velocity profile at outlet section

5.1.4 Volumetric Expansion and Rising Time

To analyze the effect of compressibility, air is considered to follow the ideal gas law. Volume rendering of air volume fraction is studied considering a small time interval to analyze the volumetric expansion of air as it flows upward. Figure 5.5 depicts the volume fraction of air at 1.4 seconds and 1.6 seconds. The tip of the air is monitored between the time interval of 1.4 seconds and 1.6 seconds. A significant amount of expansion of air at 1.6 seconds is observed compared to the air at 1.4 seconds (see Figure 5.5). The travelling time of air through the pressure cell can be determined by tracking the air volume fraction. Influx of air into the pressure cell is observed at t=1.075 seconds (see Figure 5.6). After travelling through the pressure cell, the air starts to flow through the outlet section at t=1.7375 seconds. A total of 0.73 seconds of travelling time is observed for the air from the gas inlet section to the outlet section.

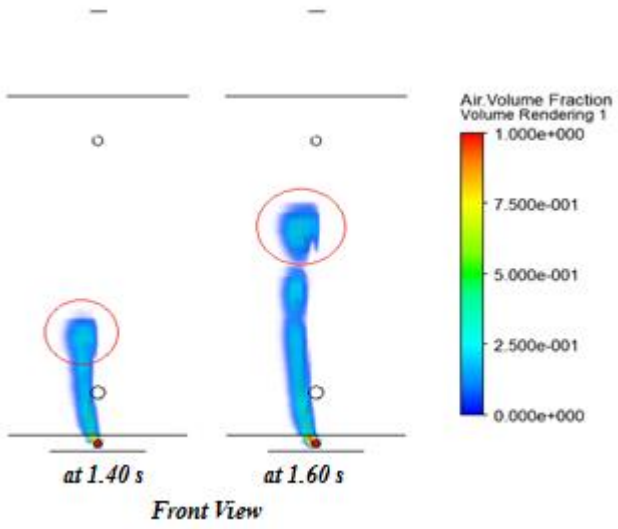

Figure 5-6 Volumetric expansion of air

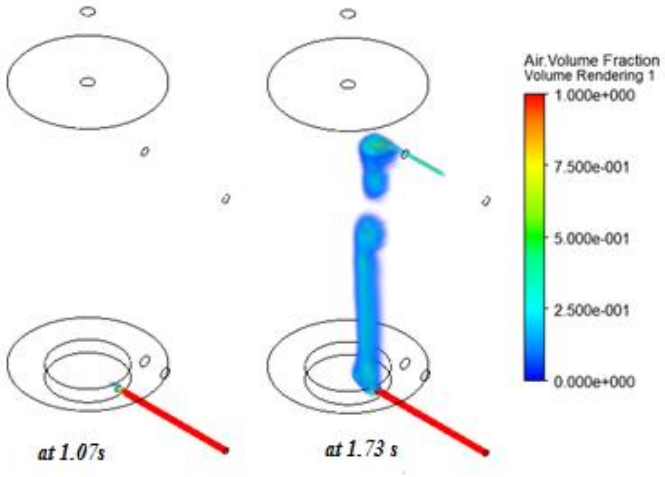

Figure 5-7 Travelling time of air into the pressure cell.

5.1.5 Discussion

The risk of casing failure due to a sudden increase of the downhole pressure due to a gas kick significantly escalates the underwater blowout risk. The simulation results of a gas kick in a scaled down version of a wellbore exhibit an increase of a considerable amount of downhole pressure. Discrete flow velocity of considered phases as an immiscible mixture is observed when the velocity profile at the outlet section is analyzed. Air flows comparatively faster than the water in the outlet section, which signifies the challenge of the quickest implementation of appropriate well control techniques. Analyzing the travelling time of a gas kick through a full scale wellbore can provide an improved insight on the quickest implementation of well control techniques. Furthermore, detection of a kick at the downhole becomes crucial when only the volume flow rate at the outlet is considered because of the observed volumetric expansion behaviour of the compressed air while flowing through the wellbore.

This study describes a successful dynamic simulation of a gas kick in a scaled down version of a wellbore. Exhaustive analysis of hydrodynamic behaviour of drilling fluid in the annulus during an influx into the wellbore is possible using numerical simulation. Analyzing the results of the numerical simulation of a gas kick in a wellbore, the following conclusions can be summarized:

- Validation of the numerical result with experimental results exhibits a close match in error ranging between 0 to 20 percentages, during the stabilized flow pattern.
- Significant change in downhole pressure is observed during an artificial kick. Numerical results exhibit a similar trend of downhole pressure increase which is observed simultaneously during the experiment.
- Discrete flow velocity is observed for air and water while flowing through the outlet section as an immiscible mixture. The high flow velocity of air compared to the water illustrates the challenge of fast response and quickest well control techniques.
- Air remains compressed at the bottom of the pressure cell and starts to expand volumetrically as it flows upward. The compressibility of gas kick at downhole describes the importance of monitoring hydrodynamic properties such as density, electrical conductivity and pressure at the bottom of the wellbore.
- 0.73 seconds of travelling time is observed for air to flow from the gas inlet to the outlet section in a scaled down version of the wellbore. Full scale wellbore simulation during a kick can provide a realistic estimation of travelling time of a kick from the formation layer.

5.2 Analysis of Risk Assessment Model

A generalized overview of data processing and incorporation of data set into the risk assesment model is presented in Figure 5.8. The data set for the primary events are monitored and recorded while the experiment is conducted. Kalman filtration method is used for noise reduction. The filtered data set for each primary event is used for developing the corresponding cumulative distribution function using Equation 7. Probability estimation for primary events are done using cumulative distribution function and threshold values for primary events and then used in risk assessment model.

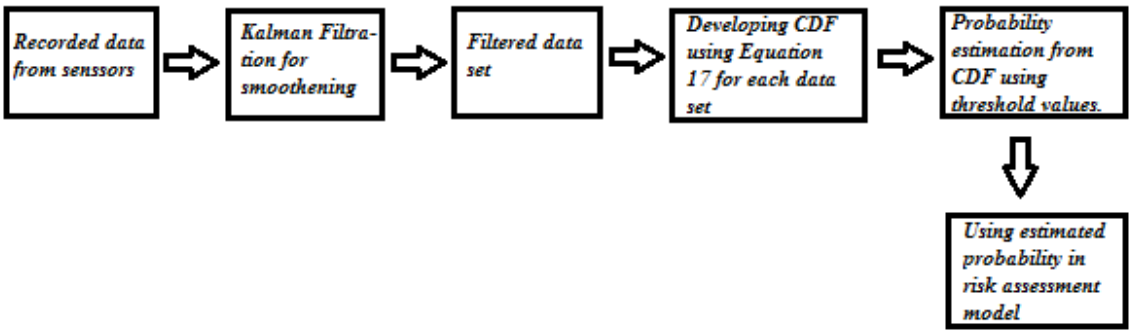

Figure 5-8 Flow diagram showing generalized overview of data process for risk assessment model.

5.2.1 Experimental Probability Calculation

To validate the risk assessment model based on four parameters, the probability of kick or influx into the system is quantified experimentally. Quantification of the experimental probability of kick is done by a gas flow meter, which detects the airflow rate into the pressure cell adjusted by the pressure regulator. Any value of gas flow rate above a safe operational limit is considered as kick and can be directly measured by a gas flow meter. The gas flow meter detects the experimental kick occurrence. The cumulative distribution

of airflow rate for each set of the experiment run is calculated by using Equation 17, where p provides the probability of each observation (each reading of the airflow at a discrete time) from a normal distribution with standard distribution $\sigma = \sqrt{\frac{1}{N-1}\sum_{i=1}^{N}(x_i - \mu)^2}$ and mean $\mu = \frac{1}{N}\sum_{i=1}^{N} x_i$.

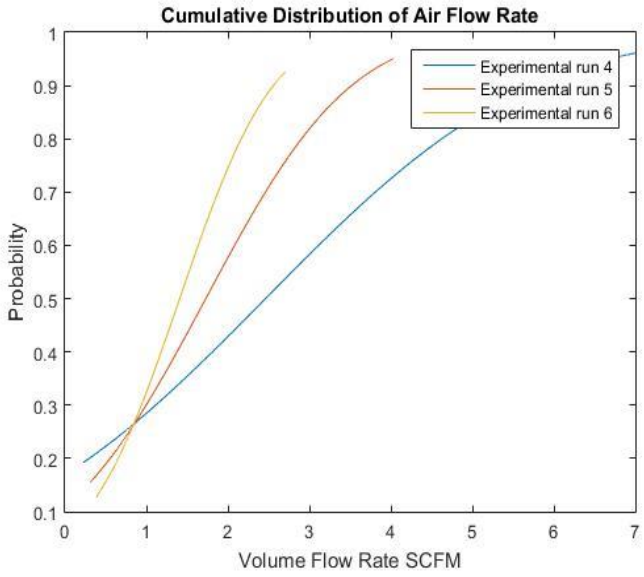

Figure 5-9 Cumulative distribution of air volume flow rate

$$p = F(x|\mu,\sigma) = \frac{1}{\sigma\sqrt{2\pi}}\int_{-\infty}^{x} e^{-\frac{(t-\mu)^2}{2\sigma^2}}dt \qquad (17)$$

Figure 5.9 delineates the cumulative distribution of the airflow rate for three sets of the experiment in second step. Probability of an experimental kick (the condition violating the safe operational limit) is demonstrated in Table 5.1 for each experimental run. The cumulative distribution of airflow rate of Experimental run 4 in Figure 5.9 shows that the probability of an airflow rate greater than 0.8 SCFM is 0.73. Analogous probabilities of airflow rates crossing a safe operational limit for Experimental runs 5 and 6 are presented

in Table 5.1. Experimental probabilities of kick for Experimental runs 5 and 6 are 0.78 and 0.80 respectively.

Table 5-1 Experimental Probability of Kick

Experiment Set	Condition	Probability
4	Pr (air flow rate > 0.80 SCFM)	0.730
5	Pr (air flow rate > 0.80 SCFM)	0.780
6	Pr (air flow rate > 0.80 SCFM)	0.800

5.2.2 Probability Calculation of Downhole Parameters

This section discusses the probability calculation of downhole parameters or primary events 1, 2, 3 and 4 in the bowtie risk assessment model in Figure 4.6. The cumulative distribution of downhole parameters for three sets of experimental runs 4, 5 and 6 are plotted in Figure 5.8 using Equation 17. In Experiment run 4, the cumulative distribution of the mass flow rate ranges between 3000 lb/hr to 4500 lb/hr. Probability of a mass flow rate greater than the safe operational limit of 3580 lb/hr (see Table 5.2) is calculated from the corresponding cumulative distribution of Experimental run 4, which is 0.54. Probabilities of the mass flow rate crossing the safe operational limit in Experimental runs 5 and 6 are measured from the corresponding cumulative distribution (Figure 5.9) and presented in Table 5.2. Cumulative distribution of pressure, density and electrical

conductivity for three runs of the experiments are also plotted in Figure 5.10. The cumulative distribution function in Figure 5.10 and safe operational limits of pressure, density and electrical conductivity presented in Table 3.1 are taken into account to assess the probability of downhole parameters violating the safe operational limit. Table 5.2 describes the probability of primary events for each experimental run. The probabilities of downhole pressure for Experiment runs 4, 5 and 6 are 0.75, 0.79 and 0.79 respectively. The probability of density and electrical conductivity are also presented in Table 5.2 for three experimental runs.

Table 5-2 Probability of downhole parameters

Index	Primary Events	Condition	Probability		
			Experimental run 4	Experimental run 5	Experimental run 6
1	Flow rate	Pr (Flow rate > Safe operational limit)	0.540	0.650	0.600
2	Downhole Pressure	Pr (Downhole Pressure > Safe operational limit)	0.750	0.790	0.790
3	Density	Pr (Density < Safe operational limit)	0.730	0.780	0.800
4	Electrical Conductivity	Pr (Electrical Conductivity < Safe operational limit)	0.700	0.800	0.820

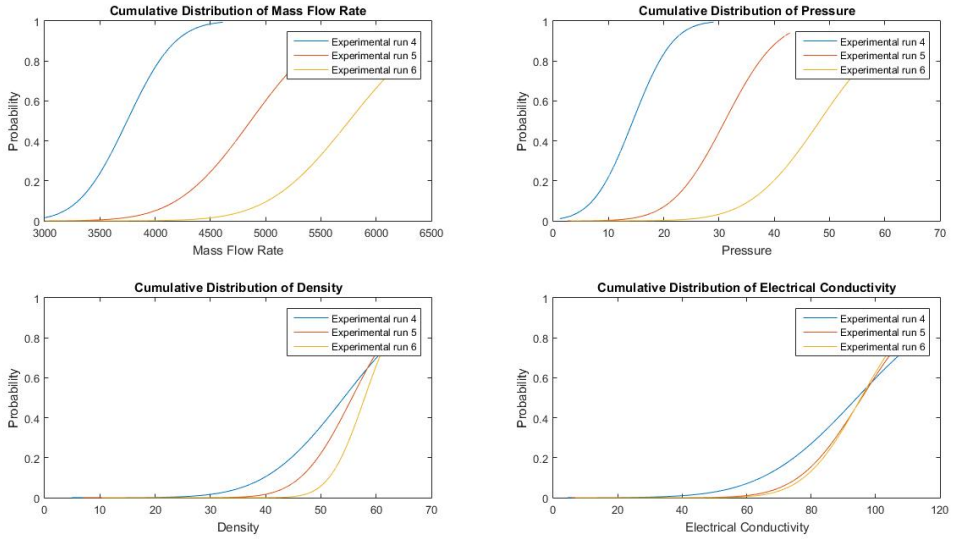

Figure 5-10 Cumulative distribution of downhole parameters

5.2.3 Validation of Kick Detection

The probability of kick is quantified experimentally (Table 5.2) to validate the kick detection part in the blowout risk assessment model. The kick detection part or the fault tree in the bowtie risk assessment model (see Figure 4.6) can be arranged by numerous scenarios of logical combinations as described in Table 4.1. Each scenario represents a unique logical combination. For example, when four events are combined using only OR logic, it is considering the case where kick is detected whenever any of the four primary events occurs. Basing kick detection on any one of the primary events increases the chance of a Type I error (false positive); similarly, when four events are combined through only AND logic, this considers the case where kick is detected when all four primary events occur. Basing kick detection on such conditions increases changes in the Type II error (false positive). A range of scenarios is tested using probability of primary events in different experiment runs. Results are presented Tables 5 3.

In Scenario 1, any single parameter including mass flow rate, downhole pressure, density or the electrical conductivity crossing a safe operational limit estimates the highest probability (0.99) of kick detection. It is significantly higher compared to experimental probability of kick (0.73). This confirms that kick detection based on at least any one of the primary events occurring overestimates kick detection. Primary events are arranged using only the AND logical expression in Scenario 2. Scenario 2 provides exact opposite result of Scenario 1.

Table 5-3 Analysis of selected scenarios of logical combinations for kick detection in Table 4.1 (Figure 4.6)

Scenario	Probability of kick					
	Experimental run 4		Experimental run 5		Experimental run 6	
	Numerical	Experimental	Numerical	Experimental	Numerical	Experimental
1	0.990	0.730	0.996	0.775	0.9969	0.805
2	0.206	0.730	0.318	0.775	0.310	0.805
3	0.813	0.730	0.885	0.775	0.883	0.805
4	0.452	0.730	0.574	0.775	0.600	0.805
5	0.372	0.730	0.49	0.775	0.456	0.805
6	**0.709**	**0.730**	**0.815**	**0.775**	**0.810**	**0.805**
7	0.940	0.730	0.972	0.775	0.971	0.805
8	0.951	0.730	0.978	0.775	0.981	0.805
9	0.803	0.730	0.886	0.775	0.889	0.805
10	0.471	0.730	0.5693	0.775	0.586	0.805
11	0.352	0.730	0.495	0.775	0.442	0.805
12	**0.718**	**0.730**	**0.814**	**0.775**	**0.813**	**0.805**
13	0.930	0.730	0.970	0.775	0.973	0.805
14	0.953	0.730	0.977	0.775	0.978	0.805
15	0.803	0.730	0.883	0.775	0.885	0.805
16	0.459	0.730	0.582	0.775	0.595	0.805
17	0.364	0.730	0.482	0.775	0.461	0.805
18	**0.712**	**0.730**	**0.817**	**0.775**	**0.816**	**0.805**
19	0.941	0.730	0.971	0.775	0.971	0.805
20	0.950	0.730	0.979	0.775	0.980	0.805

To obviate the error estimation of kick, four parameters are selected and combined in numerous ways for the rest of the scenarios. From Scenario 3 to 8, mass flow rate and downhole pressure are coupled as primary events 1 and 2. Density and electrical conductivity are coupled as primary events 3 and 4. Numerical estimation of the probability of kick for Scenario 6 is 0.709 (Experimental run 4), which exhibits almost the same value as the experimentally observed probability of kick (0.730). In scenario 6, either any combinations of mass flow rate and downhole pressure or density or electrical conductivity violating the safe operational limit estimates the kick detection. Experimental runs 5 and 6 demonstrate resemblance to Experimental run 4 for Scenario 6. Scenarios 6, 12 and 18 are the reverberation of similar logical combinations where almost analogous accuracy is observed. In Scenario 12, mass flow rate and electrical conductivity are combined and selected as primary events 1 and 2. Density and downhole pressure are coupled as primary events 3 and 4. For exhaustive analysis of kick detection 15 more logical combinations of kick detection parameters are analyzed and compared in Appendix C Table IV. The comparison between numerical and experimental results in Appendix C Table IV presents that if density is monitored individually accurate estimation of kick is possible.

5.2.4 Sensitivity Analysis

Determination of the primary events having the most crucial impact on kick detection can be done from the validated kick detection model. Scenario 12 in Table 5.3 is selected, as it provides the closest correspondence when compared to the experimental result. To determine the primary events having the most crucial impact, each primary event is

changed individually and separately at constant intervals (5%, 10%...) of percentage change to maintain uniformity of change. In Scenario 12, Pr (Flow Rate) and Pr (Electrical Conductivity) are combined through AND logic.

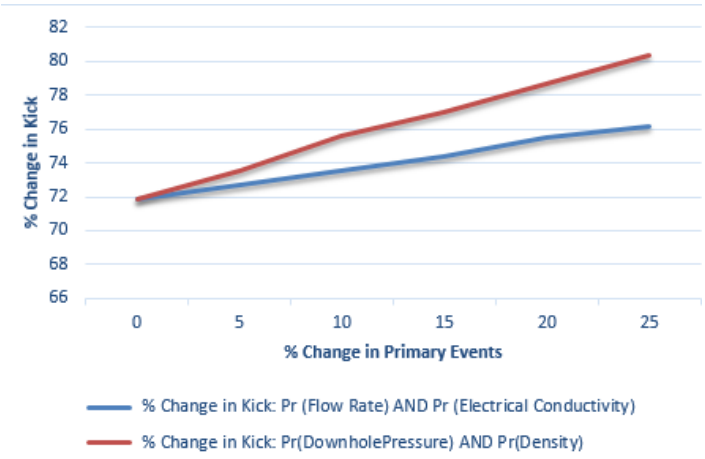

Figure 5-11 Sensitivity analysis of downhole parameters

As a result, the percentage change of kick corresponds to the percentage change of the Pr (Flow Rate) and the percentage change of Pr (Electrical Conductivity) merges. Similar scenario is observed in the case of Pr (Downhole Pressure) and Pr (Density). In Figure 5.11, percentage change in kick because of Pr (Flow Rate) and Pr (Electrical Conductivity) are presented by the same curve. Pr (Downhole Pressure) and Pr (Density) show comparatively higher impact on the percentage change of kick.

5.2.5 Time Dependency Analysis of Kick Detection

To analyze the impact of the duration of the experiment on the probability of downhole parameters violating a safe operational limit, the total duration of Experiment run 4 is segmented in six different time windows. In Appendix C Table I, variations on the

probability of downhole parameters crossing a safe operational limit according to the change of the window length are presented. As expected, the lowest probability of downhole parameters crossing a safe operational limit is observed between the time intervals of 0-60 seconds. The probability of downhole parameters starts to increase as soon as the influx is injected into the pressure cell. Probability of airflow rate or experimental probability of kick reaches a maximum of 0.764 at 0-140 seconds of the time window. Appendix C Table I exhibits that the response of kick by individual downhole parameters is unlikely to be similar and consistent with the experimental probability of kick. For exhaustive analysis of kick detection 11 new scenarios of logical combinations for downhole parameters are analyzed in Appendix C Table II. New scenarios and combinations are compared with experimental kick estimation. Combinations of any two, any three or all four parameters by AND logical expression are not likely to provide consistent accurate estimation of kick with the change of time windows. Possible scenarios of logical combinations listed in Table 4.1 are analyzed and compared with the experimental estimation of kick in Appendix C Table III. Combinations 6, 12 & 18 are likely to predict an almost accurate estimation of kick with the change of time intervals. Combination 6, 12 & 18 exhibit that any two of four parameters need to be combined and estimated together for almost accurate estimation of kick. The next accurate estimation of kick can be observed by using combinations 3, 9 and 15. The precise estimation of kick detection is observed through combinations 6, 12 & 18 for durations of 0-140 seconds.

5.2.6 Blowout Risk Assessment

Kick detection is considered most significant in the blowout risk assessment model described in Figure 4.6. To reduce the false alarm of blowout consequences, the validated kick detection pattern from Table 5.3 is adapted in the risk assessment model. The well barriers to control a kick are not included in the experimental setup, so failure probabilities of the basic events of safety barriers in the event tree are adapted from literature [34],[36],[51]. Failure probabilities of the basic events of the event tree are listed in Table 5.4. The categorized blowout consequences described in Table 4.2 are quantified on the basis of the experimentally validated kick detection model using adapted failure probabilities from literature. Barrier failure probabilities and a quantitative analysis of blowout consequences are presented in Table 5.5 and Table 5.6 respectively. The risk assessment of blowout consequences in Figure 4.6 depicts that 'disaster', having a probability of 1.03E-4, is the second most possible consequence. The probability of 'near miss' (7.05E-1) is highest compared to other consequences presented in Table 5.6.

Table 5-4 Probability of failure of basic events in Fig 4.6

Basic event	Description	Probability
5	Failure in mixing right density	2.00E-04
6	Pump failure	4.00E-04
7	Lower pipe ram	1.00E-04
8	Upper pipe ram	1.00E-04
9	Pump failure	4.00E-04
10	Choke valve failure	2.50E-04
11	Failure in mixing right density	2.00E-04
12	Pump failure	4.00E-04
13	Failure in mixing right density	2.00E-04
14	Choke valve failure	2.50E-04
15	Pump failure	4.00E-04
16	Annular Preventer	1.00E-04
17	Blind/shear ram	1.00E-04
18	Barite plug (assumed)	1.00E-04
19	Cement plug (assumed)	1.00E-04

Table 5-5 Barrier failures probability

Index	Barrier	Probability of failure
1	Casing (assumed)	2.00E-04
2	Primary well control	1.99E-04
3	secondary well control	2.30E-03
4	Blowout preventer	1.99E-04
5	Tertiary well control	1.99E-04

Table 5-6 Quantitative analysis of consequences

Index	Consequences	BT
1	Near Miss	7.05E-01
2	Mishap	4.24E-04
3	Incident	9.77E-07
4	Accident	1.95E-10
5	Disaster	1.03E-04

5.2.7 Discussion

A comparison of the kick detection model (the fault tree of bowtie analysis) with experimental results illustrates that only a few specific scenarios of logical combinations can reduce a false alarm of kick detection as well as blowout consequences. Kick detection by any of four downhole parameters violating safe operational limits will provide maximum possibility of overestimation. Overestimation refers to the over prediction of kick by the risk analysis model compared to the experimentally estimated kick. Scenarios 7, 8, 13, 14, 19 and 20 also overestimate the probability of kick, where one or two of four downhole parameters violating the safe operation limit will overestimate the probability of kick.

The opposite tendency is observed when all four parameters are combined and considered to exceed the safe operational limit. The logical condition in Scenario 2 demonstrates that

kick detection by every single downhole parameter crossing the safe operational limit will underestimate the occurrence of kick. Underestimation indicates the under prediction of kick by risk analysis model compared to the experimentally estimated kick. Underestimation of kick detection is also observed for 8 distinct scenarios of logical combinations (Scenarios 4, 5, 10, 11, 16, 17). The analysis of Scenarios 4, 5, 10, 11, 16 and 17 can be summarized as any three of four downhole parameters crossing the safe operational limit will underestimate the probability of kick.

In validated scenario 6, flow rate and downhole pressure are combined by the AND logical expression, while AND logical expression is used to combine electrical conductivity and density. Scenarios 12 and 18 depict analogous trends to Scenario 6. Similar logical conditions are repeated in Scenarios 12 and 18, where the primary events are alternated. A logical combination of Scenarios 6, 12 and 18 demonstrates that combined estimation of any two downhole parameters crossing the safe operational limit are likely to provide a reliable estimate of kick. A statement can be made that the false alarm in kick detection as well as blowout consequences are independent of the sequence of basic events but directly related to the sequence and combination of logic gates. Unlike Scenarios 6, 12 and 18, the next nearest accurate estimation of kick is observed for Scenarios 3, 9 and 15. The logical combination used in Scenarios 3, 9 and 15 demonstrates that any of those two downhole parameters crossing a safe operational limit are likely to provide an accurate estimation of kick. Accurate estimation of kick is also possible when density is monitored individually (Appendix C Table IV). Observing validated scenarios a statement can be made that if one kick detection parameter is to be monitored then density is the best choice to make, if

multiple parameters are to be monitored then logical combinations 6, 12 & 18 are best. Since the kick detection parameters act differently with the type of hydrocarbon as kick, so it is recommended to use multiple kick detection parameter to detect kick. Furthermore, the sensitivity analysis of basic events depicts that the occurrence as well as timeliness of kick is somewhat prone to downhole pressure and density.

5.3 Synopsis

Comparison of numerical simulation (CFD) results with experimental observations and flow pattern analysis exhibits a close match. Significant change in downhole pressure and discrete velocity of air and water are observed. Volumetric expansion of gas is obvious as air tends to flow through the pressure cell. Validation and analysis of kick detection fault tree exhibits that an accurate estimation of kick compared to the experimental results is possible when multiple parameters are monitored and combined with specific logical scenarios. Furthermore, time dependency analysis exhibits an on time risk estimation of kick. The probability of kick predicted my risk estimation model changes with respect to time.

Chapter 6

6 Conclusion

This thesis is focused on the numerical simulation of the change of hydrodynamic property during a kick prior to the blowout consequences. Furthermore, a risk assessment model of blowout consequences based on real time process data is developed. Both numerical model and risk assessment model are compared and validated with experimentally obtained results. The numerical simulation part of the work is submitted in the Journal of Petroleum Science and Engineering on the title of 'Numerical Simulation and Experimental Validation of Kick to Analyze Well Blowout Risk'. The risk assessment part of the work is submitted in Reliability Engineering and Safety Science on the title of 'Well Blowout Risk Assessment Model Testing and Validation'.

Numerical simulation results are compared and validated with experimental studies at first and then an exhaustive analysis of simulation results are done to examine the hydrodynamic property change during an influx. Obtained numerical results exhibit a quite a good match with experimental results having a maximum twenty percentage of error during stabilized condition. Volumetric expansion of gaseous phase while travelling upward as well as discrete flow velocity of two immiscible mixtures are obvious, which are analyzed through numerical simulation.

Blowout risk assessment model is proposed based on the bow tie approach where kick detection is considered as the key element. The kick detection part of the blowout risk assessment model is tested and validated using a downhole experimental setup. Around 35 percent of an overestimation of kick detection may result when any one of the four parameters violating a safe operational limit is considered. On the contrary, 71 percent of underestimation of kick detection is observed when all four parameters are combined and all four parameters are considered as having crossed the safe operational limit. The study concludes that kick detection is reliably estimated while any two out of four parameters are combined and considered to violate a safe operational limit. In Scenarios 6, 12 & 18 mass flow rate is coupled with downhole pressure, electrical conductivity and density respectively. In other words, reliable estimation is possible when mass flow rate is combined with any three parameters and is considered to have crossed safe operational limit. Analyzing the validated scenarios of logical combination, it is important to note that a false alarm of kick detection as well as blowout consequences are independent of the sequence of primary events but are directly related to the sequence and combination of logic gates. The kick occurrence is used along with adopted data from previous studies to estimate the consequences of blowout risk analysis.

This work can be further improved by overcoming the bowtie shortcomings such as the common cause of failure, causation dependence and also inability to update blowout prediction based on real time observation of well control barriers. A Bayesian network is highly recommended as a possible approach for risk analysis of these improvements. The Bayesian network model can be developed and integrated with real time monitoring of well

conditions. This will provide a reliable real time risk estimate. To model consequence, the loss function approach may be considered. On time risk estimation of kick and visualization as well as blowout consequences are possible when the proposed validated model is coded in Matlab and synchronized with Labview. Furthermore the validation of event tree part of the risk assessment model is possible depending upon the availability of experimental studies on well control techniques. The proposed numerical model can be further extended for full scale wellbore considering appropriate phase as an influx. Rotational motion of drill string as well as heat transfer between phases can be incorporated for more realistic and practical prediction of hydrodynamic property change in a wellbore during a kick.

Appendix-A

Scalar form of conservation equations:

$$\frac{\partial \rho}{\partial t} + \frac{\partial}{\partial t}(\rho v_x) + \frac{\partial}{\partial t}(\rho v_y) + \frac{\partial}{\partial t}(\rho v_z) = 0$$

Momentum equation in x direction:

$$\frac{\partial}{\partial t}(\rho v_x) + \frac{\partial}{\partial x}(\rho v_x v_x) + \frac{\partial}{\partial y}(\rho v_y v_x) + \frac{\partial}{\partial z}(\rho v_z v_x) = -\frac{\partial p}{\partial x} + \frac{\partial}{\partial x}\left[\lambda \nabla . \vec{v} + 2\mu \frac{\partial v_x}{\partial x}\right] + \frac{\partial}{\partial y}\left[\mu(\frac{\partial v_x}{\partial y} + \frac{\partial v_y}{\partial x}\right] + \frac{\partial}{\partial z}\left[\mu(\frac{\partial v_x}{\partial z} + \frac{\partial v_z}{\partial x}\right] + \rho g_x$$

Momentum equation in y direction:

$$\frac{\partial}{\partial t}(\rho v_y) + \frac{\partial}{\partial x}(\rho v_x v_y) + \frac{\partial}{\partial y}(\rho v_y v_y) + \frac{\partial}{\partial z}(\rho v_z v_y) = -\frac{\partial p}{\partial y} + \frac{\partial}{\partial y}\left[\lambda \nabla . \vec{v} + 2\mu \frac{\partial v_y}{\partial y}\right] + \frac{\partial}{\partial x}\left[\mu(\frac{\partial v_y}{\partial x} + \frac{\partial v_x}{\partial y}\right] + \frac{\partial}{\partial z}\left[\mu(\frac{\partial v_y}{\partial z} + \frac{\partial v_z}{\partial y}\right] + \rho g_y$$

Momentum equation in z direction:

$$\frac{\partial}{\partial t}(\rho v_z) + \frac{\partial}{\partial x}(\rho v_x v_z) + \frac{\partial}{\partial y}(\rho v_y v_z) + \frac{\partial}{\partial z}(\rho v_z v_z) = -\frac{\partial p}{\partial z} + \frac{\partial}{\partial z}\left[\lambda \nabla . \vec{v} + 2\mu \frac{\partial v_z}{\partial z}\right] + \frac{\partial}{\partial x}\left[\mu(\frac{\partial v_z}{\partial x} + \frac{\partial v_x}{\partial z}\right] + \frac{\partial}{\partial y}\left[\mu(\frac{\partial v_z}{\partial y} + \frac{\partial v_y}{\partial z}\right] + \rho g_z$$

Appendix-B

```
#include "udf.h"
DEFINE_PROFILE(inlet_mf,th,i)
{
face_t f;
begin_f_loop(f,th)
{
if(CURRENT_TIME <= 0.9)
F_PROFILE(f,th,i) = 0;
else if(CURRENT_TIME <=1 && CURRENT_TIME >0.9)
F_PROFILE(f,th,i) = 0.000065024/2.2;
else if(CURRENT_TIME <=1.1 && CURRENT_TIME >1)
F_PROFILE(f,th,i) = 0.000115646/2.2;
else if(CURRENT_TIME <=1.2 && CURRENT_TIME >1.1)
F_PROFILE(f,th,i) = 0.000143846/2.2;
else if(CURRENT_TIME <=1.3 && CURRENT_TIME >1.2)
F_PROFILE(f,th,i) = 0.00017608/2.2;

- - - - - - - - - - - - - - - - - - - - - - - - - - - - - - - - - - - - - - - -

- - - - - - - - - - - - - - - - - - - - - - - - - - - - - - - - - - - - - - - -

- - - - - - - - - - - - - - - - - - - - - - - - - - - - - - - - - - - - - - - -
}
end_f_loop(f,th);
}
```

Appendix-C

Table I Time dependent probability of downhole parameters crossing safe operational limit

Time Interval	0-60 seconds	0-80 seconds	0-100 seconds	0-120 seconds	0-140 seconds	0-161 seconds
A | Flow Rate	0.325	0.490	0.646	0.707	0.666	0.540
B | Downhole Pressure	0.272	0.536	0.677	0.745	0.739	0.750
C | Density	0.532	0.509	0.664	0.739	0.750	0.730
D | Electrical Conductivity	0.500	0.457	0.600	0.692	0.724	0.700
E | Airflow Rate (Experimental)	0.379	0.589	0.709	0.773	0.764	0.730

Table II Time dependency of logical scenarios for kick detection

Time Interval	Probability of kick											
	0-60 seconds		0-80 seconds		0-100 seconds		0-120 seconds		0-140 seconds		0-161 seconds	
Combination	Numerical	Experimental	Numerical	Experimental	Numerical	Experimental	Numerical	Experimental	Numerical	Experimental	Numerical	Experimental
AB	0.088	0.379	0.263	0.589	0.437	0.709	0.527	0.773	0.492	0.764	0.405	0.730
AC	0.173	0.379	0.249	0.589	0.429	0.709	0.522	0.773	0.499	0.764	0.394	0.730
AD	0.162	0.379	0.224	0.589	0.388	0.709	0.489	0.773	0.482	0.764	0.378	0.730
BC	0.145	0.379	0.273	0.589	0.449	0.709	0.550	0.773	0.554	0.764	0.548	0.730
BD	0.136	0.379	0.245	0.589	0.406	0.709	0.515	0.773	0.535	0.764	0.525	0.730
CD	0.266	0.379	0.232	0.589	0.398	0.709	0.511	0.773	0.542	0.764	0.511	0.730
ABC	0.047	0.379	0.134	0.589	0.290	0.709	0.389	0.773	0.369	0.764	0.296	0.730
BCD	0.072	0.379	0.125	0.589	0.270	0.709	0.381	0.773	0.401	0.764	0.383	0.730
ACD	0.086	0.379	0.114	0.589	0.257	0.709	0.362	0.773	0.361	0.764	0.276	0.730
ABD	0.044	0.379	0.120	0.589	0.262	0.709	0.365	0.773	0.356	0.764	0.284	0.730
ABCD	0.023	0.379	0.061	0.589	0.174	0.709	0.269	0.773	0.267	0.764	0.207	0.730

Table III Time dependency of logical scenarios (Table 4.1) for kick detection

Time Interval	Probability of kick											
	0-60 seconds		0-80 seconds		0-100 seconds		0-120 seconds		0-140 seconds		0-161 seconds	
Index	Numerical	Experimental	Numerical	Experimental	Numerical	Experimental	Numerical	Experimental	Numerical	Experimental	Numerical	Experimental
Comb-1	0.885	0.379	0.937	0.589	0.985	0.709	0.994	0.773	0.994	0.764	0.990	0.730
Comb-2	0.023	0.379	0.061	0.589	0.174	0.709	0.269	0.773	0.267	0.764	0.206	0.730
Comb-3	0.389	0.379	0.560	0.589	0.766	0.709	0.851	0.773	0.850	0.764	0.813	0.730
Comb-4	0.135	0.379	0.177	0.589	0.353	0.709	0.473	0.773	0.495	0.764	0.452	0.730
Comb-5	0.068	0.379	0.193	0.589	0.378	0.709	0.484	0.773	0.458	0.764	0.372	0.730
Comb-6	**0.331**	**0.379**	**0.434**	**0.589**	**0.661**	**0.709**	**0.769**	**0.773**	**0.768**	**0.764**	**0.709**	**0.730**
Comb-7	0.639	0.379	0.819	0.589	0.931	0.709	0.963	0.773	0.960	0.764	0.940	0.730
Comb-8	0.786	0.379	0.803	0.589	0.924	0.709	0.962	0.773	0.965	0.764	0.951	0.730
Comb-9	0.436	0.379	0.558	0.589	0.765	0.709	0.849	0.773	0.848	0.764	0.803	0.730
Comb-10	0.096	0.379	0.197	0.589	0.386	0.709	0.501	0.773	0.503	0.764	0.471	0.730
Comb-11	0.107	0.379	0.173	0.589	0.346	0.709	0.457	0.773	0.450	0.764	0.352	0.730
Comb-12	**0.283**	**0.379**	**0.436**	**0.589**	**0.663**	**0.709**	**0.770**	**0.773**	**0.769**	**0.764**	**0.718**	**0.730**
Comb-13	0.711	0.379	0.799	0.589	0.922	0.709	0.959	0.773	0.959	0.764	0.930	0.730
Comb-14	0.714	0.379	0.823	0.589	0.933	0.709	0.966	0.773	0.966	0.764	0.953	0.730
Comb-15	0.435	0.379	0.561	0.589	0.767	0.709	0.851	0.773	0.850	0.764	0.803	0.730
Comb-16	0.093	0.379	0.184	0.589	0.358	0.709	0.476	0.773	0.490	0.764	0.459	0.730
Comb-17	0.110	0.379	0.187	0.589	0.373	0.709	0.481	0.773	0.463	0.764	0.364	0.730
Comb-18	**0.285**	**0.379**	**0.433**	**0.589**	**0.661**	**0.709**	**0.769**	**0.773**	**0.767**	**0.764**	**0.712**	**0.730**
Comb-19	0.727	0.379	0.811	0.589	0.929	0.709	0.963	0.773	0.961	0.764	0.941	0.730
Comb-20	0.699	0.379	0.811	0.589	0.926	0.709	0.962	0.773	0.964	0.764	0.950	0.730

Table IV Analysis of scenarios of logical combinations for kick detection

A | Flow Rate
B | Downhole Pressure
C | Density
D | Electrical Conductivity

Scenario	Probability of kick					
	Experimental run 4		Experimental run 5		Experimental run 6	
	Numerical	Experimental	Numerical	Experimental	Numerical	Experimental
A	0.540	0.730	0.650	0.775	0.600	0.805
B	0.750	0.730	0.790	0.775	0.790	0.805
C	**0.730**	**0.730**	**0.780**	**0.775**	**0.800**	**0.805**
D	0.700	0.730	0.800	0.775	0.820	0.805
AB	0.405	0.730	0.514	0.775	0.474	0.805
AC	0.394	0.730	0.507	0.775	0.480	0.805
AD	0.378	0.730	0.520	0.775	0.492	0.805
BC	0.548	0.730	0.616	0.775	0.632	0.805
BD	0.525	0.730	0.632	0.775	0.648	0.805
CD	0.511	0.730	0.624	0.775	0.656	0.805
ABC	0.296	0.730	0.401	0.775	0.379	0.805
ACD	0.276	0.730	0.406	0.775	0.394	0.805
ABD	0.284	0.730	0.411	0.775	0.389	0.805
BCD	0.383	0.730	0.493	0.775	0.518	0.805
ABCD	0.207	0.730	0.320	0.775	0.311	0.805

Appendix-D

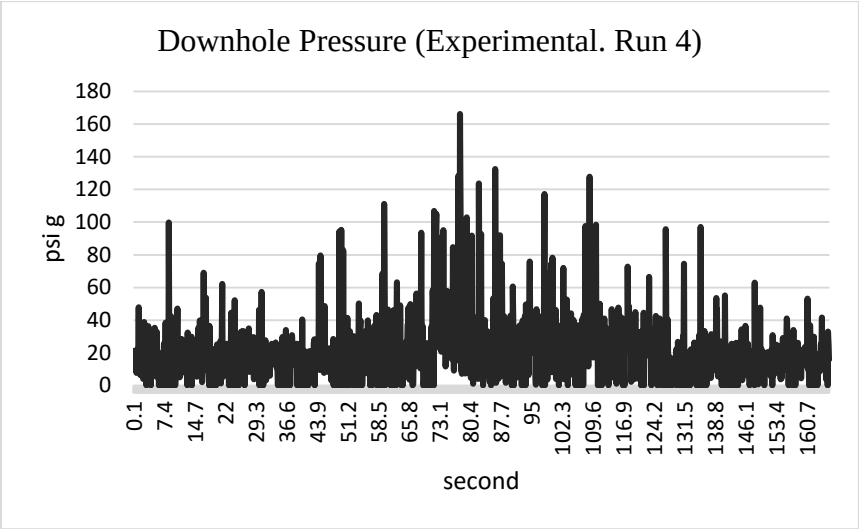

Figure I Change of downhole pressure (Prior Kalman filtration)

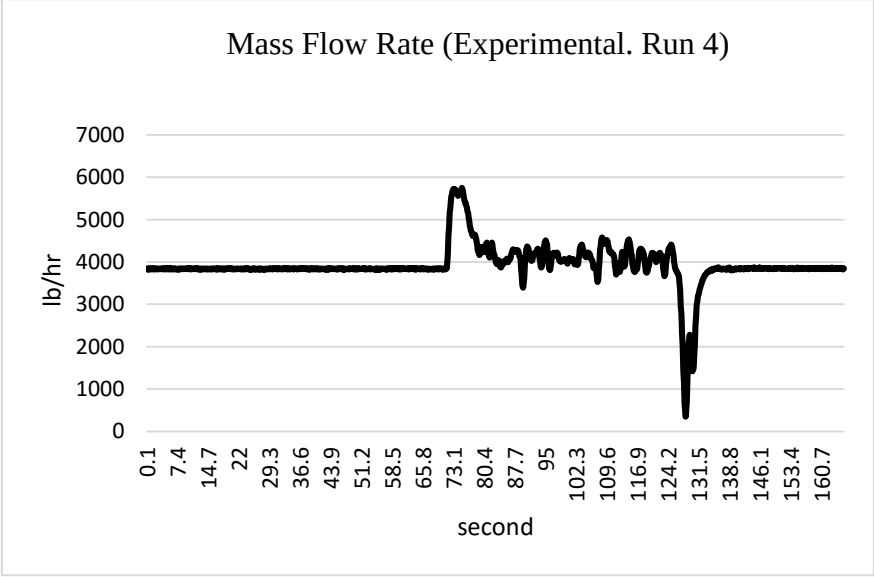

Figure II Change of mass flow rate (Prior Kalman filtration)

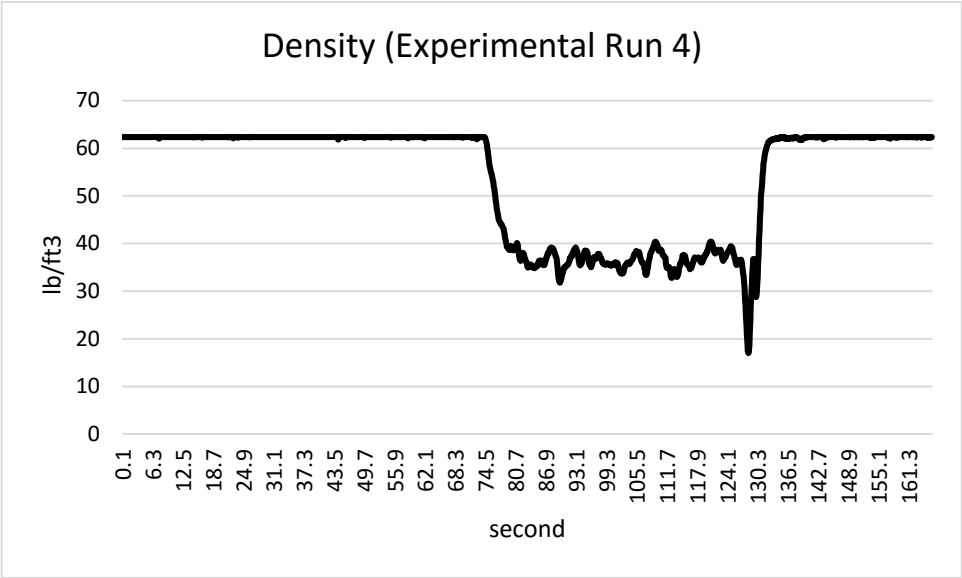

Figure III Change of density (Prior Kalman filtration)

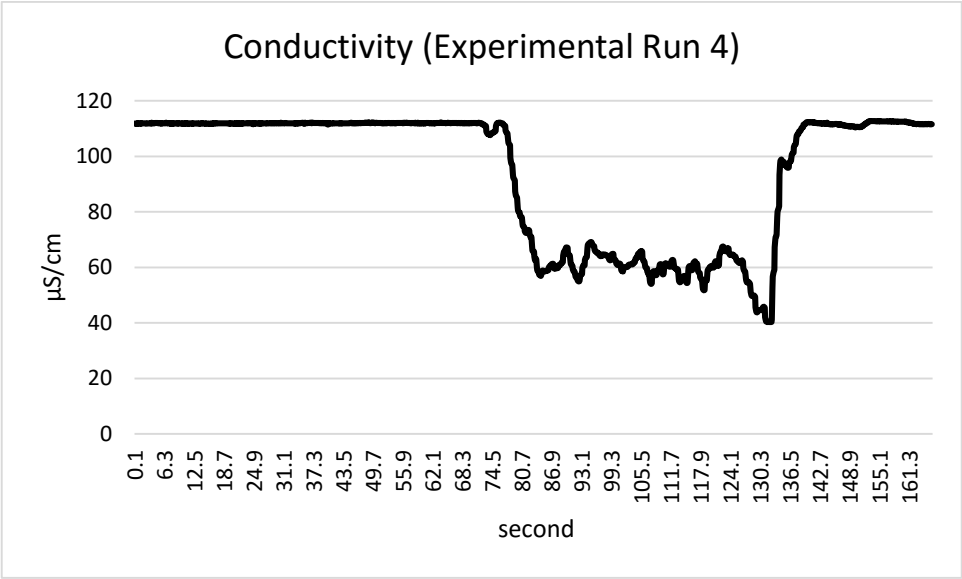

Figure IV Change of conductivity (Prior Kalman filtration)

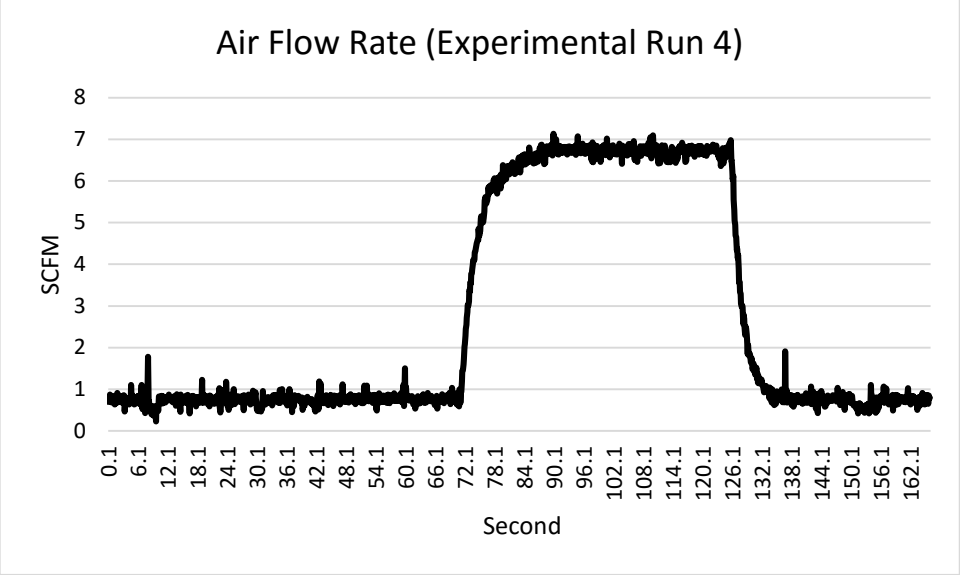

Figure V Change of air flow rate (Prior Kalman filtration)

References

[1] Guo B., Liu G. Applied Drilling Circulation Systems - Hydraulics, Calculations, and Models. *Elsevier*. 2011

[2] Lake, L. W., Fanchi, J. R. Petroleum Engineering Handbook. *Society of Petroleum Engineers*. 2005

[3] Grace, R. D. Blowout and Well Control Handbook. *Elsevier*. 2003

[4] Mitchell, R. F., Miska, S. Z. Fundamentals of Drilling Engineering. *Society of Petroleum Engineers*. 2010

[5] Ahmed, T. Reservoir Engineering Handbook. *Elsevier*. 2006

[6] N. Khakzad, F. Khan and P. Amyotte. Dynamic safety analysis of process systems by mapping bow- tie into Bayesian network. *Process Safety and Environmental Protection 91(1-2),* pp. 46-53. 2013. DOI: 10.1016/j.psep.2012.01.005.

[7] K. Ling, J. He, J. Ge, P. Pei and Z. Shen. A rigorous method to calculate the rising speed of gas kick. *Journal of Petroleum Exploration and Production Technology 5(1),* pp. 81-89. 2015. DOI: 10.1007/s13202-014-0111-4.

[8] Leblanc, J. L., & Lewis, R. L. A mathematical model of a gas kick. *Society of Petroleum Engineers*. August 1, 1968. DOI: 10.2118/1860-PA

[9] Nickens, H. V. A dynamic computer model of a kicking well. *Society of Petroleum Engineers*. June 1, 1987. DOI: 10.2118/14183-PA

[10] Nunes, J. O. L., Bannwart, A. C., & Ribeiro, P. R. Mathematical modeling of gas kicks in deep water scenario. *Society of Petroleum Engineers*. January 1, 2002. DOI: 10.2118/77253-MS

[11] Petersen, J., Rommetveit, R., Bjorkevoll, K. S., & Froyen, J. A general dynamic model for single and multi-phase flow operations during drilling, completion, well control and intervention. *Society of Petroleum Engineers*. January 1, 2008. DOI: 10.2118/114688-MS

[12] Perez-Tellez, C., Smith, J. R., & Edwards, J. K. A new comprehensive, mechanistic model for underbalanced drilling improves wellbore pressure predictions. *Society of Petroleum Engineers.* January 1, 2002. DOI: 10.2118/74426-MS

[13] Gomez, L. E., Shoham, O., Schmidt, Z., Chokshi, R. N., Brown, A., & Northug, T. A unified mechanistic model for steady-state two-phase flow in wellbores and pipelines. *Society of Petroleum Engineers*. January 1, 1999. DOI: 10.2118/56520-MS

[14] Ansari, A. M., Sylvester, N. D., Shoham, O., & Brill, J. P. A comprehensive mechanistic model for upward two-phase flow in wellbores. *Society of Petroleum Engineers*. January 1, 1990. DOI: 10.2118/20630-MS

[15] Lage, A. C. V. M., Fjelde, K. K., & Time, R. W. Underbalanced drilling dynamics: two-phase flow modeling and experiments. *Society of Petroleum Engineers*. January 1, 2000. DOI: 10.2118/62743-MS

[16] C. S. Avelar, P. R. Ribeiro and K. Sepehrnoori. Deepwater gas kick simulation. *Journal of Petroleum Science and Engineering 67(1–2),* pp. 13-22. 2009.

[17] J. Xie, X. Zhang, Y. Tang, Y. Wang, Q. Shao and B. Yu. Transient simulation of the blowing-out process of the air pockets in vertical wellbore. *Appl. Therm. Eng. 72(1),* pp. 97-103. 2014.

[18] Mona Golbabaei-Asl, Alex Povitsky and Lev Ring. CFD Modeling of fast transient processes in drilling fluid. *Proc. ASME.* 57465, *Volume 7A: Fluids Engineering Systems and Technologies*, November 13, 2015. DOI: 10.1115/IMECE2015-52482.

[19] A. Ambrus, U. J. F. Aarsnes, A. Karimi Vajargah, B. Akbari, E. van Oort and O. M. Aamo. Real-time estimation of reservoir influx rate and pore pressure using a simplified transient two-phase flow model. *Journal of Natural Gas Science and Engineering 32*pp. 439-452. 2016.

[20] Rajnish K Kalay, Arne E Holdo. CFD modelling of multiphase flows-an overview. *Proc. ASME.* 41510, *Emerging Technology in Fluids, Structures, and Fluid Structure Interactions*: 83-89. January 01, 2003. DOI: 10.1115/PVP2003-1951

[21] A. Coughtrie, D. Borman and P. Sleigh. Effects of turbulence modelling on prediction of flow characteristics in a bench- scale anaerobic gas- lift digester. *Bioresource technology 2013.*

[22] M. Masum Jujuly, A. Rahman, S. Ahmed and F. Khan. LNG pool fire simulation for domino effect analysis. *Reliab. Eng. Syst. Saf. 143*pp. 19-29. 2015.

[23] ANSYS Fluent Theory Guide. Release 14.0. November 2011.

[24] Anderson Jr, J. D. "Governing equations of fluid dynamics." *Computational fluid dynamics*. Springer Berlin Heidelberg, 2009. 15-51.

[25] B. Sun, K. Guo and V. K. Pareek. Computational fluid dynamics simulation of LNG pool fire radiation for hazard analysis. *J Loss Prev Process Ind 29*pp. 92-102. 2014.

[26] Florian R. Menter. Turbulence modelling for engineering flows. 2011 ANSYS, Inc (Technical paper 25).

[27] R. Lanzafame, S. Mauro and M. Messina. 2D CFD modeling of H-darrieus wind turbines using a transition turbulence model. *Energy Procedia 45*pp. 131-140. 2014.

[28] F. R. Menter, R. B. Langtry, S. R. Likki, Y. B. Suzen, P. G. Huang and S. Völker. A correlation-based transition model using local Variables—Part I: Model formulation. *Journal of Turbomachinery 128(3),* pp. 413-422. 2004.

[29] S. Yakubov, T. Maquil and T. Rung. Experience using pressure-based CFD methods for Euler–Euler simulations of cavitating flows. *Comput. Fluids 111*pp. 91-104. 2015

[30] A. A. Nayeem, R. Venkatesan and F. Khan. Monitoring of down-hole parameters for early kick detection. *Journal of Loss Prevention in the Process Industries 40*pp. 43-54. 2016.

[31] ANSYS Fluent UDF Manual. Release 15.0. November 2013

[32] B. Cai, Y. Liu, Z. Liu, X. Tian, Y. Zhang and R. Ji. Application of Bayesian networks in quantitative risk assessment of subsea blowout preventer operations. *Risk Analysis 33(7),* pp. 1293-1311. 2013. DOI: 10.1111/j.1539-6924.2012.01918.x.

[33] A. Nouri.Gharahasanlou, A. Mokhtarei, A. Khodayarei and M. Ataei. Fault tree analysis of failure cause of crushing plant and mixing bed hall at khoy cement factory in Iran. *Case Studies in Engineering Failure Analysis 2(1),* pp. 33-38. 2014. DOI: 10.1016/j.csefa.2013.12.006.

[34] A. L. FG Bercha and. Probabilities of Blowouts in Canadian Arctic Waters: A Report 1978.

[35] J. E. Skogdalen and J. E. Vinnem. Quantitative risk analysis of oil and gas drilling, using Deepwater Horizon as case study. *Reliability Engineering & System Safety 100*pp. 58-66. 2012.

[36] N. Khakzad, F. Khan and P. Amyotte. Quantitative risk analysis of offshore drilling operations: A Bayesian approach. *Safety Science 57*pp. 108-117. 2013.

[37] B. Ale, D. Hanea, C. van Gulijk, P. Lin and P. Hudson. Towards an integrated risk model for hydrocarbon industry operation. *Advances in Safety, Reliability and Risk Management: ESREL 2011* pp. 258. 2011.

[38] J. Bhandari, R. Abbassi, V. Garaniya and F. Khan. Risk analysis of Deepwater drilling operations using Bayesian network. *Journal of Loss Prevention in the Process Industries 38*pp. 11-23. 2015.

[39] L. Xue, J. Fan, M. Rausand and L. Zhang. A safety barrier- based accident model for offshore drilling blowouts. *Journal of Loss Prevention in the Process Industries 26(1),* pp. 164-171. 2013. DOI: 10.1016/j.jlp.2012.10.008.

[40] V. Vandenbussche, A. Bergsli., H. Brandt, O. W. W. Brude, and T. R. Nissen-lie, (2012, January 1). Well-specific Blowout Risk Assessment. *Society of Petroleum Engineers*. doi:10.2118/157319-MS

[41] SINTEF Offshore Blowout Database-Chapter Four 1997. DOI: 10.1016/B978-088415514-0/50006-6.

[42] J. Weiss. Deep water drilling risk reduction assessment. *Mide Technology Corporation*. Boston Avenue. 2010

[43] L. B. Andersen. Stochastic modelling for the analysis of blowout risk in exploration drilling. *Reliability Engineering and System Safety 61(1),* pp. 53-63. 1998. DOI: 10.1016/S0951-8320(97)00067-7.

[44] N. Ramzali, M. R. M. Lavasani and J. Ghodousi. Safety barriers analysis of offshore drilling system by employing fuzzy event tree analysis. *Safety Science 78*pp. 49-59. 2015.

[45] O. Arild, E. P. Ford, T. Loberg, and J. W. T. Baringbing, (2009, January 1). Kick Risk—A Well Specific Approach to the Quantification of Well Control Risks. *Society of Petroleum Engineers*. doi:10.2118/124024-MS.

[46] L. A. Ritchie, D. A. Gill, R. T. Sylves and L. K. Comfort. The exxon valdez and BP deepwater horizon oil spills. *American Behavioral Scientist 56(1),* pp. 76-103. 2012. DOI: 10.1177/0002764211413116.

[47] L. A. Carlsen, G. Nygaard and M. Nikolaou. Evaluation of control methods for drilling operations with unexpected gas influx. *J. Process Control*. DOI: 10.1016/j.jprocont.2012.12.003.

[48] D. Fraser, R. Lindley, D. D. Moore, and M. V. Staak, (2014, October 27). Early Kick Detection Methods and Technologies. *Society of Petroleum Engineers*. doi:10.2118/170756-MS

[49] N. Khakzad, F. Khan and P. Amyotte. Dynamic safety analysis of process systems by mapping bow- tie into bayesian network. *Process Safety and Environmental Protection 91(1-2),* pp. 46-53. 2013. DOI: 10.1016/j.psep.2012.01.005.

[50] J. E. Skogdalen, I. B. Utne and J. E. Vinnem. Developing safety indicators for preventing offshore oil and gas deepwater drilling blowouts. *Safety Science 49(8–9),* pp. 1187-1199. 2011.

[51] M. Abimbola, F. Khan, N. Khakzad and S. Butt. Safety and risk analysis of managed pressure drilling operation using bayesian network. *Safety Science 76*pp. 133-144. 2015.

[52] E. Hauge. Automatic kick detection and handling in managed pressure drilling systems. Ph.D. dissertation, Department of Engineering Cybernetics, Norwegian University of Science and Technology, Trondheim, 2013

[53] NORSOK standard: Well integrity in drilling and well operations. D-010 Norwegian Technology Center, NORSOK (2004).

[54] P. Holand. Offshore Blowouts: Causes and Control 1997.

[55] R. D. Grace. Blowout and Well Control Handbook 2003.

[56] S. Rathnayaka, F. Khan and P. Amyotte. SHIPP methodology: Predictive accident modeling approach. part I: Methodology and model. *Process Safety and Environmental Protection* 151-164,pp. 2011.

[57] A. A. Nayeem, R. Venkatesan and F. Khan. Monitoring of down-hole parameters for early kick detection. *Journal of Loss Prevention in the Process Industries 40*pp. 43-54. 2016.

[58] G. Welch, G. Bishop, "An Introduction to the Kalman Filter",University of North Carolina at Chapel Hill Department of Computer Science, 2001.